Phylogenetic profiling and cellular analyses of ARL16 reveal roles in traffic of IFT140 and INPP5E

Skylar I. Dewees[a,b], Romana Vargová[c], Katherine R. Hardin[b,d], Rachel E. Turn[a,b,e], Saroja Devi[a], Joshua Linnert[f], Uwe Wolfrum[f], Tamara Caspary[g], Marek Eliáš[c], and Richard A. Kahn[a,*]

[a]Department of Biochemistry, [d]Department of Cell Biology, and [g]Department of Human Genetics, Emory University School of Medicine, Atlanta, GA 30322; [b]Biochemistry, Cell & Developmental Biology Graduate Program, Laney Graduate School, Emory University, Atlanta, GA 30307; [c]Department of Biology and Ecology, Faculty of Science, University of Ostrava, CZ-710 00, Ostrava, Czech Republic; [e]Department of Microbiology and Immunology, Stanford University, Palo Alto, CA 94305-5124; [f]Institute of Molecular Physiology, Johannes Gutenberg University, Mainz 55128, Germany

ABSTRACT **The ARF family of regulatory GTPases is ancient, with 16 members predicted to have been present in the last eukaryotic common ancestor. Our phylogenetic profiling of paralogues in diverse species identified four family members whose presence correlates with that of a cilium/flagellum: ARL3, ARL6, ARL13, and ARL16. No prior evidence links ARL16 to cilia or other cell functions, despite its presence throughout eukaryotes. Deletion of ARL16 in mouse embryonic fibroblasts (MEFs) results in decreased ciliogenesis yet increased ciliary length. We also found *Arl16* knockout (KO) in MEFs to alter ciliary protein content, including loss of ARL13B, ARL3, INPP5E, and the IFT-A core component IFT140. Instead, both INPP5E and IFT140 accumulate at the Golgi in *Arl16* KO lines, while other intraflagellar transport (IFT) proteins do not, suggesting a specific defect in traffic from Golgi to cilia. We propose that ARL16 regulates a Golgi–cilia traffic pathway and is required specifically in the export of IFT140 and INPP5E from the Golgi.**

Monitoring Editor
Fanni Gergely
University of Cambridge

Received: Oct 21, 2021
Revised: Jan 11, 2022
Accepted: Feb 18, 2022

INTRODUCTION

ARF family regulatory GTPases are best known for their roles in regulating bidirectional membrane traffic throughout the secretory pathway, including at Golgi and endosomes (Sztul *et al.*, 2019). However, they also regulate a diverse array of other pathways and functions, including at cilia (Fisher *et al.*, 2020), mitochondria, lipid droplets, centrioles, midbodies, and rods and rings (Sztul *et al.*, 2019). To achieve such widespread cellular regulation, mammals express as many as 30 ARF family GTPases, including six ARFs, 22 ARF-like (ARL), two SARs, and TRIM23. Like all regulatory GTPases, they switch between "inactive" (GDP-bound) and "active" (GTP-bound) conformations in response to the actions of guanine nucleotide exchange factors (GEFs) and GTPase-activating proteins (GAPs). With regulatory roles in such diverse and essential cellular processes, ARF family members are implicated in a large number of pathologies including cancers, ciliopathies, hearing and vision impairments, idiopathic pulmonary fibrosis, and other maladies. Despite their importance to cell biology and human health, we lack substantial mechanistic details of their actions (Sztul *et al.*, 2019). Indeed, some of the core family members remain virtually unstudied.

We recently reported the results of a taxonomically broad phylogenetic analysis of the ARF family in eukaryotes (Vargová *et al.*, 2021). This study defines the set of family members ancestral for eukaryotes and describes 16 paralogues putatively present in the last eukaryotic common ancestor. We used our large phylogenetic data set to look for the retention or loss of family members that are correlated with retention or loss of the cilium. Strikingly, as elaborated below, the phyletic pattern of ARL16 genes provided a hypothesis that its cellular function is relevant to cilia. A link between ARL16 and cilia also emerged in a CRISPR screen for regulators of

This article was published online ahead of print in MBoC in Press (http://www.molbiolcell.org/cgi/doi/10.1091/mbc.E21-10-0509-T) on February 23, 2022.

*Address correspondence to: Richard A. Kahn (rkahn@emory.edu).

Abbreviations used: Ac-Tu, acetylated tubulin; GAP, GTPase-activating protein; GEF, guanine nucleotide exchange factor; KO, knockout cell line; MEF, mouse embryonic fibroblast.

the Hedgehog signaling pathway (Breslow *et al.*, 2018). ARL16 was previously reported to be cytosolic and inhibit the function of the RIG-I protein in defense against RNA viruses (Yang *et al.*, 2011). Also, two high-throughput data sets identified potential interacting partners of ARL16, including PDE6D (aka PDE6δ or PrBP/delta) and GM130, providing additional clues to its location and functions (Rolland *et al.*, 2014; Luck *et al.*, 2020). Thus, despite some fragmentary data on ARL16 from several systems, there has been no systematic approach aimed at identifying fundamental actions of ARL16 in cells or, more specifically, in cilia.

The primary cilium is a sensory structure, responding to extracellular signals with cellular responses through complex intracellular signaling networks. Primary cilia are made up of a microtubule-based backbone, the axoneme, which extends from the modified mother centriole, termed the basal body (Satir and Christensen, 2007). The axoneme is covered in the ciliary sheath, which is continuous with the plasma membrane but functionally separated from it by the transition zone, which tightly regulates entry to the ciliary compartment (Stephen *et al.*, 2017). Three paralogues in the ARL family, ARL3, ARL6, and ARL13, play roles in ciliary functions, acting both inside and outside of cilia (Chiang *et al.*, 2004; Fan *et al.*, 2004; Zhou *et al.*, 2006; Fisher *et al.*, 2020; Gigante and Caspary, 2020). ARL3 regulates the delivery of N-myristoylated and prenylated proteins to the cilium by binding cargo transporters UNC119 and PDE6D, respectively (Fansa *et al.*, 2016; Stephen *et al.*, 2017). ARL6/BBS3 regulates the function of the BBSome (a protein complex involved in export of ciliary membrane proteins (Mourão *et al.*, 2014). ARL13, including the extensively studied mammalian paralogue ARL13B, is involved in ciliary protein import and export, partly mediated by its activity as a GEF for ARL3 (Gotthardt *et al.*, 2015; Ivanova *et al.*, 2017). It is also well known for its crucial role in vertebrate development via one of the best-known ciliary signaling pathways, Hedgehog (Hh) (Caspary *et al.*, 2007). In this pathway, Hh ligand binds to its receptor, Patched (PTCH), which is enriched on the ciliary membrane. This induces the removal of PTCH from the cilium, allowing the G protein–coupled receptor (GPCR) Smoothened (SMO) to enter (Goetz *et al.*, 2009). This leads to cleavage and activation of Gli transcription factors, which then translocate to the nucleus, resulting in the transcription of target genes. This pathway is heavily influenced by other ciliary proteins including ARL13B, ARL3, and INPP5E, often through alterations in SMO recruitment or changes in Gli activation (Caspary *et al.*, 2007; Jacoby *et al.*, 2009; Lai *et al.*, 2011). Changes in lipid metabolism are also likely involved as ARL13B directly binds both INPP5E (Qiu *et al.*, 2021), a phosphoinositide 5′-phosphatase, and ARL3, to activate it and thereby promote release of INPP5E from its transporter PDE6D.

Coordinated protein traffic to and within the cilium is essential for both its formation (ciliogenesis) and function (ciliary signaling). Small proteins (<~100 kDa) can diffuse across the barrier at the base of the cilium, the transition zone (Dishinger *et al.*, 2010; Nachury and Mick, 2019). The passage of other proteins through the transition zone is tightly controlled by the intraflagellar transport (IFT) protein complexes, IFT-A and IFT-B, and the BBSome (Lechtreck, 2015; Wingfield *et al.*, 2018). Cilium assembly and length are regulated in large part by IFT machinery, with IFT-A and IFT-B complexes involved in retrograde and anterograde traffic, respectively (Nachury, 2018; Wang *et al.*, 2021). These multisubunit complexes are required for the regulated entry and export of proteins from cilia, acting in concert with another protein complex, the BBSome, at the base of cilia in the transition zone. IFT-A is also required for efficient traffic of ciliary membrane cargoes to the cilium, acting as a vesicle coat complex between the Golgi and cilia (Quidwai *et al.*, 2021). Ciliary protein content is further regulated by targeting of newly synthesized proteins from the endoplasmic reticulum (ER) to the Golgi to the cilium and recycling of membrane proteins from the plasma membrane to the ciliary membrane through either lateral diffusion or recycling through endosomes, though these pathways are less well understood than traffic within the cilium itself (Nachury, 2018; Carter and Blacque, 2019).

To begin testing the hypothesis that ARL16 is important to ciliary biology and to search for additional roles in cell biology, we knocked out the gene in immortalized mouse embryonic fibroblasts (MEFs). These lines display defects in ciliogenesis, ciliary protein traffic, and ciliary signaling, confirming the phylogenetic prediction and experimentally linking a fourth ARL to cilia. Furthermore, the ciliary traffic defects observed in *Arl16* knockout (KO) cells appear to be linked to, and possibly the direct result of, changes in traffic of key ciliary proteins through the Golgi. Thus, these data provide an initial characterization of the cellular functions of ARL16 linked to cilia, as well as a role in protein export from the Golgi.

RESULTS

ARL16 is a divergent member of the ARF family

ARL16 is among the least characterized GTPases in the ARF family despite its predicted presence in the last eukaryotic common ancestor (Vargová *et al.*, 2021). Sequence alignments reveal ARL16 to be among the most divergent members of the family in mammals, sharing only ~27% identity to ARF1 (compared with >60% identity among the ARFs and >40% identity among most ARLs) (Supplemental Figure S1). Mammalian tissues widely express ARL16 mRNAs, based on searches of RNA and proteome databases, including NCBI Gene and GTexPortal.

ARL16's length is unusually variable among mammals, with two variants expressed in humans (Supplemental Figure S1A). The shorter human transcript (NM_001040025.3), encoding a 173 residue protein, is common among mammals, though a longer human isoform of 197 residues is also reported (NM_001040025.2). The longer variant corresponds to an mRNA starting from an upstream transcription initiation site, extending the 5′ end to include an alternative upstream initiation codon. In mice, a frame-shifting indel precludes a similar extension of the coding sequence of the ARL16 gene (unpublished data); thus mice express only the 173 residue protein. The prevalent, shorter form results in a truncated N-terminus, compared with every other ARF family member, with the G-1 motif (GXXXGKT) beginning at residue 6, in contrast to residue 24 in ARF1 (Supplemental Figure S1A). We predict that this difference in the N-terminus has potentially important functional consequences for two reasons. First, the N-termini of ARF family GTPases make direct contacts with binding partners/effectors, effectively serving as a conformationally sensitive "switch III" (Zhang *et al.*, 2009). Also, the shorter form has a cysteine at residue 2 that is predicted to be S-palmitoylated (e.g., by the online prediction tool CSS-Palm [http://csspalm.biocuckoo.org/online.php]). In contrast, the N-terminal extension in the longer isoform moves the cysteine well into the protein, where it is no longer predicted to be palmitoylated.

ARL16 proteins clearly retain most of the five "G-motifs" found in GTP-binding proteins that together are involved in nucleotide binding, conformational changes resulting from the switching between GDP and GTP binding, and nucleotide hydrolysis (Bourne *et al.*, 1991; Wittinghofer and Vetter, 2011) (highlighted in red in Supplemental Figure S1A and boxed in red in Supplemental Figure S1B). Mammalian ARL16 retains the conserved G-1 (GX_4GKT), G-2 (PTXG), and G-4 (NKXD) motifs, motifs that are involved in GXP

binding and interconversion between the active and inactive conformations as shown for ARFs (Pasqualato *et al.*, 2002) (alignment shown in Supplemental Figure S1A). In contrast, the ARL16 G-3 motif is altered from the highly conserved WDXGGQ (in which the glutamine participates directly in GTP hydrolysis) to RELGGC in ARL16 from multiple species, including humans and mice (Supplemental Figure S1, A and B). This change suggests the use of an alternative mechanism of GTP hydrolysis and presents a challenge to researchers as it lacks the glutamine (Q71 in ARFs or Q61 in RAS) in this motif that is commonly mutated to generate a "dominant activating" mutant, used to identify novel functions when expressed in cells.

The phylogenetic profile of ARL16 predicts a cilium-associated function

When examining the distribution pattern of ARL16 established by the previous analysis of 114 eukaryotic species (Vargová *et al.*, 2021), we noticed that the gene is missing from eukaryotes that lack ciliated (flagellated) cells or stages. To further assess this emerging pattern, we exploited existing genome and transcriptome assemblies to check for the presence of ARL16 orthologues in 25 additional eukaryotes (Supplemental Tables S1 and S2). The expansion of the sampling was guided by an attempt to cover representatives of additional major phylogenetic lineages of eukaryotes missing in the previous study and to include additional instances of independently evolved nonciliated taxa. This expanded analysis further supported the view of ARL16 as a broadly conserved and ancient ARF family paralogue, as virtually all major eukaryotic lineages include at least some ARL16-carrying representative (Figure 1; Supplemental Table S1). Multiple alignment of the diverse eukaryote ARL16 sequences revealed that the N-terminal truncation characteristic of the shorter human variant (see above) is in fact a rule rather than exception among ARL16 orthologues (Supplemental Figure S1B). The majority of ARL16 proteins across the eukaryotic phylogeny are predicted to be S-palmitoylated near the N-terminus (Vargová *et al.*, 2021), but many lack this modification as they do not have any cysteine residues in that region (Supplemental Figure S1B). Interestingly, the G-4 motif, critical for the specificity of binding of guanine nucleotides (Wittinghofer and Vetter, 2011), is abrogated in ARL16 proteins from several unrelated taxa (Supplemental Figure S1), suggesting that these proteins may function as ATPases (Leipe *et al.*, 2002). Overall, ARL16 appears to be a rapidly evolving ARF family subgroup with differences in its primary structure, suggesting substantial variation in the molecular details of ARL16 functioning among taxa.

In contrast to some other ancestral ARF family paralogues, ARL16 does not appear to have undergone lineage-specific gene duplications as there are few paralogues with (potentially) differentiated function. The only two taxa with more than one ARL16 gene (the rotifer *Adineta vaga* and the parabasalid *Trichomonas vaginalis* both have two paralogues) both accumulate duplicated genes due to whole-genome or massive segmental duplications, respectively (Flot *et al.*, 2013; Barratt *et al.*, 2016). Thus, the most conspicuous aspect of ARL16 evolution in eukaryotes is frequent independent loss. The distribution of ARL16 orthologues across the eukaryotic tree implies >30 independent loss events, scattered across different time points (affecting recently evolved taxa as well as ancient radiation of major eukaryotic taxa; Figure 1). Notably, the expanded sampling confirmed the initial observation that ARL16 occurs only in eukaryotes for which the ability to form cilia is directly documented or at least predicted by genomic evidence (i.e., presence of genes encoding typical ciliary proteins; Figure 1; Supplemental Table S1). The loss of ARL16 in relation to the loss of the cilium is nonrandom, with high statistical significance (best tail $p > 4 \times 10^{-6}$, pairwise comparisons as implemented in the Mesquite package; see *Materials and Methods*). However, ARL16 is also absent from various taxa that retained a cilium (Figure 1; Supplemental Table S1). On the basis of these observations, we hypothesize that the cellular role of ARL16 is related to the cilium, more specifically to be dependent on it but not necessarily essential for the function of the cilium as such. To provide a context for the putative association of ARL16 and cilia, we investigated the distribution of ARL3, ARL6, and ARL13 orthologues in the same taxa as we did for ARL16. Like ARL16, orthologues of ARL3, ARL6, and ARL13 are virtually always absent from taxa that do not form cilia (the sole exception being two highly divergent putative ARL6 orthologues in the heterolobosean *Neovahlkampfia damariscottae* that may have been recruited for a novel cilium-independent function). Thus, ARL3, ARL6, and ARL13 can be missing from ciliated taxa but this occurs less frequently than for ARL16 (Figure 1; Supplemental Table S1). Altogether, these comparative genomic analyses provide a strong case for the hypothesis that ARL16 is functionally linked to the cilium.

ARL16 localizes to primary cilia in cultured human RPE cells and photoreceptor cells of the human retina

ARL proteins frequently are found in multiple locations in cells, reflecting that a single ARL can perform multiple functions (Sztul *et al.*, 2019). ARL16 was previously found in cytosol in HEK293 and HeLa cells (Yang *et al.*, 2011). We performed immunofluorescence studies of endogenous ARL16 in MEFs and RPE1 cells. Despite the fact that the human and mouse ARL16 proteins (173 residue variant) share 86% identity, the only commercially available ARL16 antibody is specific to the human protein. Thus, we could not identify specific staining of ARL16 in MEFs or in cryosections through murine retinas (unpublished data). In contrast, staining of human retinal pigmented epithelial (hTert-RPE1 [RPE1]) cells revealed that ARL16 localizes along the ciliary axoneme in a punctate manner (Figure 2A). ARL16 also localized to both the cytosol and the mitochondria, as evidenced by its diffuse staining across the cell and colocalization with the mitochondrial protein HSP60, respectively (Supplemental Figure S2A).

To further examine the localization of ARL16 in MEFs and RPE1 cells, we generated plasmids that direct human ARL16 or mouse ARL16-myc expression. We generated homologous plasmids for the long or short form of human ARL16. Upon expression of the 173 residue human or mouse proteins in MEFs, we observed diffuse ARL16 staining in the cytosol (Supplemental Figure S2B). In contrast, the 197 residue human variant displayed little evidence of diffuse, cytosolic localization. Instead, tubular and punctate staining colocalized strongly with HSP60 at mitochondria, consistent with endogenous staining of RPE1 cells after methanol fixation (Supplemental Figure S2A). Thus, different-length human variants localize quite distinctly when exogenously expressed. Because the endogenous staining of ARL16 in RPE1 cells displays prominent mitochondrial localization, we believe that these cells express at least some of the longer form of ARL16. Despite the presence of endogenous ARL16 in cilia in RPE cells, we did not find evidence of the exogenous protein localizing to cilia in MEFs.

We also analyzed ARL16 localization in photoreceptor cells in the retina, a commonly studied ciliary model tissue. The light-sensitive outer segment resembles a highly modified but well-characterized primary cilium (Roepman and Wolfrum, 2007; May-Simera *et al.*, 2017). We used indirect immunofluorescence staining on a human donor retina as previously reported (Davidson *et al.*, 2013; Turn *et al.*, 2021, 2022). Figure 2B shows double labeling of ARL16 and centrin 3, a marker for the connecting cilium as well as the mother (basal

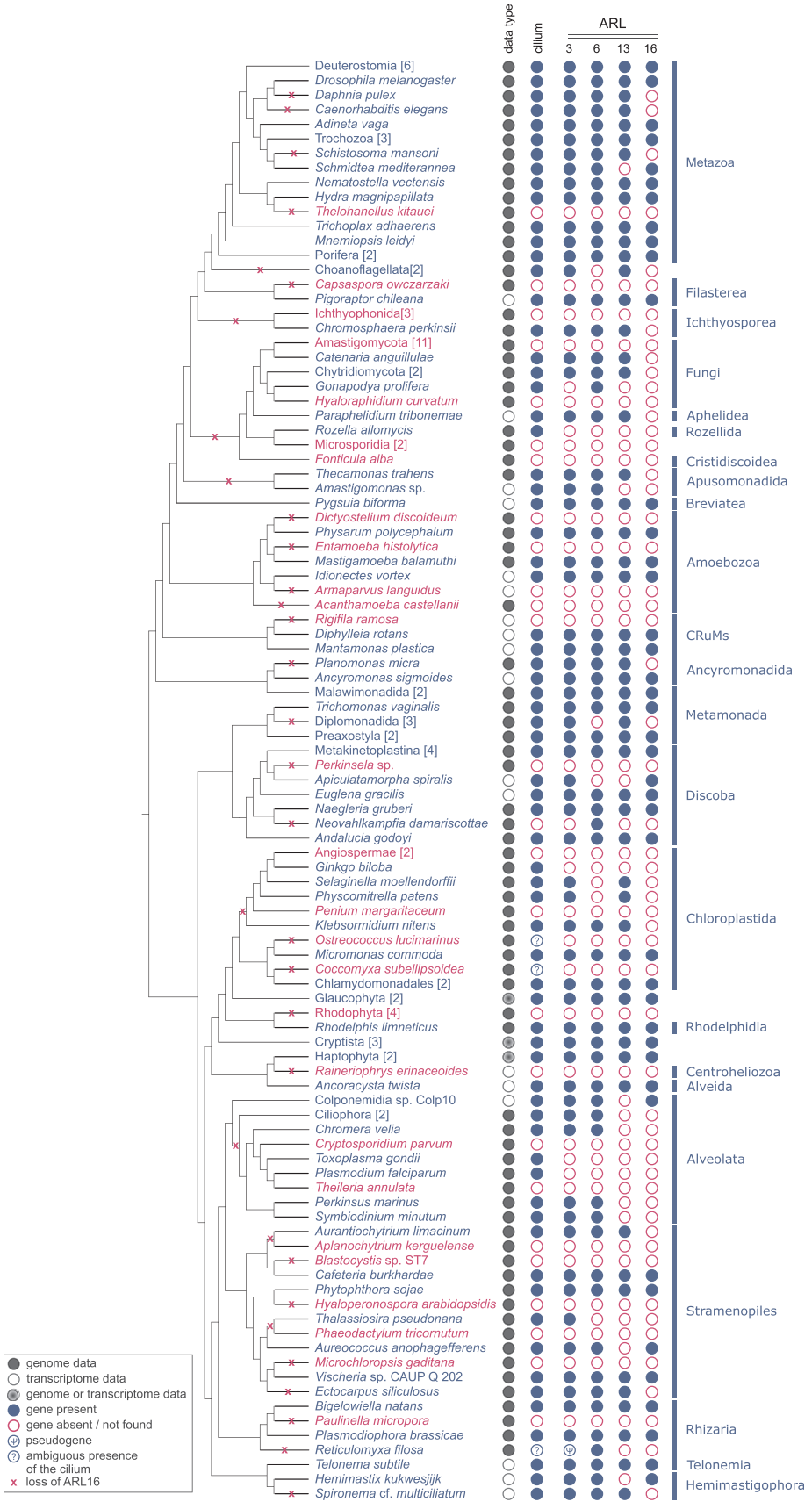

FIGURE 1: Phylogenetic distribution of ARL16 and the three previously known cilium-associated ARF family members (ARL3, ARL6, and ARL13) and cilia in eukaryotes. The distribution of the four ARF-like genes and cilium (columns) is depicted by filled blue circles (gene/cilium is present) or empty red circles (gene/cilium is absent or not detected). In three species the status of the cilium is ambiguous (see *Materials and Methods* and Supplemental Table S1). The sequence data type analyzed to establish the presence/absence of the ARLs in the different taxa are indicated ("genome or transcriptome" means that these two types of resources had to be combined to obtain a full set of the orthologues sought). The absence of any of the four ARLs in taxa represented only by transcriptome assemblies must be considered tentative, as the respective genes may be present but not expressed in the stage used for generating the transcriptome data. The schematic phylogeny on the right reflects the current state of knowledge based on multiple phylogenomic analyses. Monophyletic groups of two or more species uniform as to the presence/absence of the cilium and the four focal ARLs are shown as single branches, with the name of the respective broader taxon and the number of taxa included indicated in square brackets (see Supplemental Table S1 for the full species list). The relationship at the level of the deepest branches, still not completely settled, is adopted from a recent comprehensive phylogenomic analysis (Tice *et al.*, 2021), whereas the root of the tree is indicated following the rooting hypothesis by Derelle *et al.* (2015). Independent losses of the ARL16 gene as inferred by parsimony reasoning from its distribution of extant taxa are mapped onto the phylogenetic tree. The loss of ARL16 in relation to the loss of the cilium was tested with the Pairwise comparisons test (implemented in the Mesquite package; see *Materials and Methods*) and is nonrandom with high statistical significance (best tail $p > 4 \times 10^{-6}$).

body) and daughter centrioles of photoreceptor cells in human retinas. Prominent ARL16 immunofluorescence labeled the ciliary region (CR) and the inner segment of the photoreceptor layer. Other retinal layers, such as the outer and inner nuclear layers (ONL, INL), the outer and inner plexiform layers (OPL, IPL) where retinal synapses are localized, and the ganglion cell layer (GCL), showed no substantial staining. Higher magnification of the ciliary region revealed the localization of ARL16 in the periciliary region at the base of the connecting cilium (stained by anti–centrin 3) in human photoreceptor cells (Figure 2B, bottom panels). The centrin 3 costaining further showed that ARL16 labeled the basal body next to the daughter centriole. The inner segment where all biosynthetic active organelles such as the Golgi and ER are found also showed prominent ARL16 immunofluorescence. Similar localizations were previously found for ciliary molecules that participate in Golgi functions and/or Golgi and molecular trans-

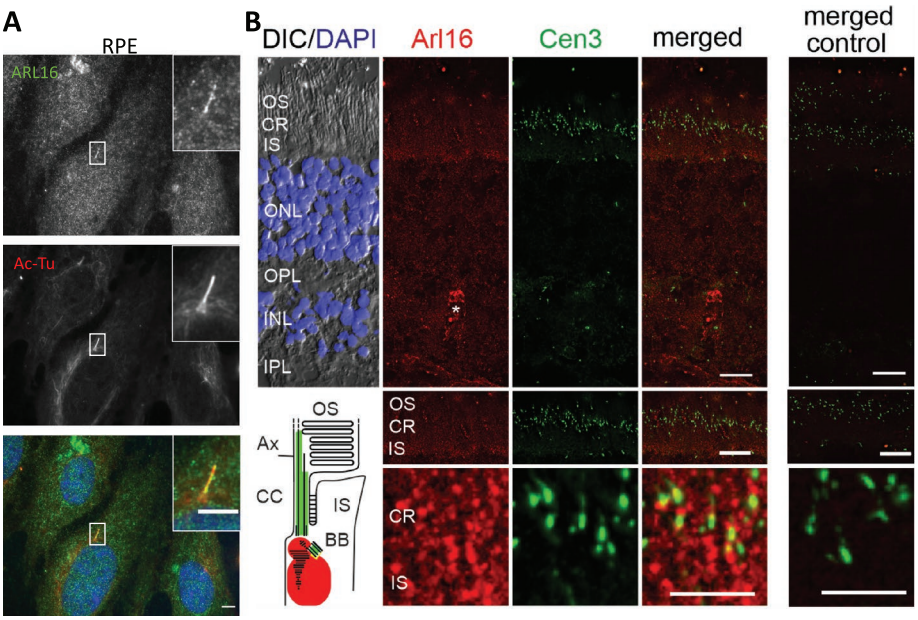

FIGURE 2: Characterization of endogenous ARL16 localization in RPE1 cells and human retina. (A) ARL16 localizes to cilia in RPE1 cells, as observed by immunocytochemistry after PFA fixation (see *Materials and Methods)*. RPE1 cells were serum starved for 48 h and stained for ARL16 (green), Ac-Tu (red), and Hoechst (blue). (B) Indirect coimmunolabeling of ARL16 (red) and centrin 3 (green), a common marker for the connecting cilium (CC) and the basal body (BB), of a human retina revealed immunofluorescence of ARL16 in the ciliary region (CR) and the inner segment (IS) of retinal photoreceptor cells. Photoreceptor outer segments (OS), DAPI-stained outer and inner nuclear layers (blue, ONL, INL), and outer and inner plexiform layers (OPL, IPL) did not show substantial staining. Asterisk (*) indicates anti-ARL16 blood vessel staining. No staining was observed in controls lacking ARL16 antibodies. Scheme of ARL16 localization in photoreceptor cells. ARL16 is localized to periciliary/basal body region (BB) and in the IS of human photoreceptor cells. Scale bars: A, 10 μm; B, 15 and 5 μm (higher magnification).

fer processes to the ciliary base (Sedmak and Wolfrum, 2010). The localization at the base of the connecting cilium is in line with other GTPases of the ARF superfamily like ARL2 and the ARF GAP ELMOD2, which also localize to ciliary rootlets in the inner segment (Turn *et al.*, 2021).

CRISPR/Cas9 KO of *Arl16* in MEFs

To test the prediction of a role for ARL16 in ciliary function, and to assess broader questions of its function in cells, we used CRISPR/Cas9 to introduce frame-shifting mutations into the open reading frame of *Arl16* in MEFs. These cells are frequently used in cell biological studies, easily imaged due to their flat morphology, commonly used in cilia research, and diploid (which facilitates genome editing analyses). We used two guides to target Cas9 to exon 2, just downstream of the ATG that is present near the end of exon 1 in *Arl16*, and screened clonal lines for indels by DNA sequencing of targeted regions. We sought frame-shifting mutations predicted to cause premature translation termination and loss of protein function. The lack of a mouse antibody precluded us from directly testing for the absence of protein expression. Although there is strong evidence (Smits *et al.*, 2019) that cells may express mutated proteins resulting from use of downstream start sites or alternative splicing, the small size of the *Arl16* open reading frame and the presence of multiple, essential G-motifs along the length of the protein (highlighted in red in Supplemental Figures S1 and S3) make expression of a functional protein after introduction of indels near the N-terminus highly unlikely. We also analyzed the potential for alternative splicing to generate a truncated, but potentially functional, protein and found that no such splicing variants would be in frame or functional (Supplemental Figure S3). Similarly, the use of the next potential initiating methionine would also generate a highly truncated protein that lacks essential motifs for activity (Supplemental Figure S3). Thus, we refer to these as KO lines. We generated five *Arl16* KO clonal lines from two different guides that we used in these studies (alleles are shown in Supplemental Figure S3A). Because we found only minor differences between the KO lines, the data are presented in aggregate. As a further test of specificity and to ensure against off-target effects influencing our phenotyping, we performed rescue experiments in which we exogenously expressed ARL16-myc in KO and wild-type (WT) lines and assessed the reversal of phenotypes arising from the KOs.

Because almost nothing is known about ARL16 functions, and to obtain an unbiased overview of the effect of ARL16 loss on cells, we screened markers of major organelles and the cytoskeleton to look for any large differences between the *Arl16* KO lines and the parental WT MEFs. No obvious differences were observed in mitochondrial morphology or distribution (HSP60), F-actin (FITC-phalloidin), nuclear number, size, or morphology (Hoechst), or microtubule networks (α/β-tubulin) when cells were fixed and stained as indicated (Supplemental Figure S3B), though we acknowledge that more detailed analyses of these structures may reveal changes. However, screening using other organelle markers revealed a number of cellular defects in *Arl16* KO lines, which we describe below.

Arl16 KO cells have reduced ciliation and increased ciliary length

In light of the phylogenetic prediction of a role for ARL16 at cilia and its localization there, we examined *Arl16* KO cilia. We used acetylated tubulin (Ac-Tu) staining throughout to mark the ciliary axoneme after inducing ciliation in cultured cells. All five of the *Arl16* null lines displayed reductions in the percentage of ciliated cells, compared with WT MEFs (Figure 3, A and B). We also quantified the percentage of ciliated cells using IFT88 to mark cilia, to protect against the possibility that changes in tubulin acetylation may skew interpretations and obtained a similar result (Supplemental Figure S4I). When the data from the five KO lines were pooled, the KOs had ~50% as many ciliated cells as WT after 24 h. However, at later time points the differences between WT and KO lines decreased, down to ~25% lower at 72 h of serum starvation and without reaching statistical significance. Thus, there is a decrease in ciliation compared with WT.

To ensure that the changes in ciliation were due to the loss of ARL16 and not off-target effects, we expressed ARL16-myc in WT and *Arl16* KO cells. One day after transfection, we serum starved for 24 h and scored the percentage ciliation in cells expressing ARL16-myc. Interestingly, the percentage of WT cells with cilia increased

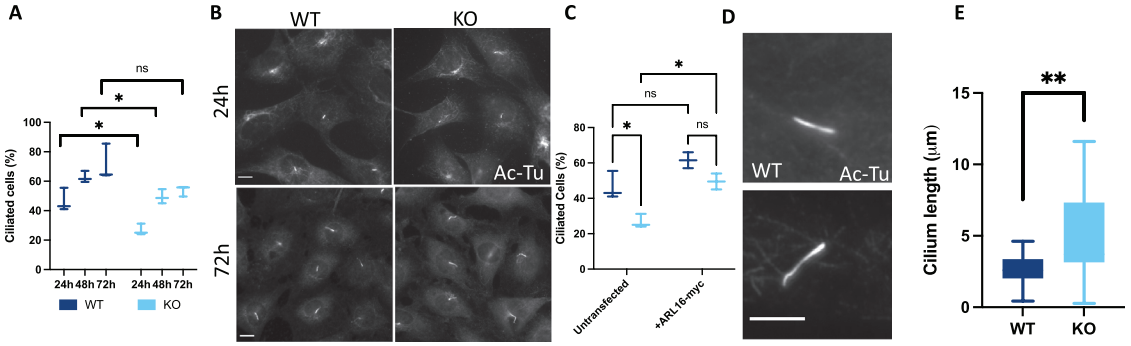

FIGURE 3: Deletion of *Arl16* causes defects in ciliogenesis. (A) WT and *Arl16* KO MEFs were serum starved with percentage of ciliated cells manually counted. For each cell line ($N = 2$ WT and 5 KO), 100 cells were scored at each time point in triplicate and averaged. Mean, Min, and Max plotted for each time point. Multiple unpaired *t* tests, false discovery rate Q = 1%, two-stage step-up method of (Benjamini, Krieger, and Yekutieli). 24 h $p = 0.017503$, 48 h $p = 0.020865$, 72 h $p = 0.076598$. (B) *Arl16* KO cells fail to ciliate as efficiently as WT cells, particularly at earlier time points after serum starvation. WT and *Arl16* KO MEFs serum starved for 24 or 72 h and stained for Ac-Tu. Scale bar = 10 μm, 60×. (C) Expression of ARL16-myc restores ciliation in *Arl16* KO cells after 24 h of serum starvation. Values for untransfected cells are equivalent to the data from panel A at 24 h of serum starvation. Ciliation of transfected cells was scored as in panel A ($N = 2 \times 50$ transfected cells from one WT line and two KO lines). Mean, Min, and Max plotted for each condition. Two-way ANOVA Tukey's multiple comparisons (untransfected WT vs. KO $p = 0.0315$, WT transfected vs. untransfected $p = 0.1349$, KO untransfected vs. transfected $p = 0.0277$, transfected WT vs. KO $p = 0.3133$). (D) *Arl16* KO cilia are longer than WT cilia. Cells were serum starved for 48 h before fixing and staining for Ac-Tu and imaged at 100×. Scale bar = 5 μm. (E) Cilium lengths were measured in WT and *Arl16* KO cells using the CiliaQ plug-in in FIJI. $N = 26$ cilia for one WT and two KO lines. *t* test $p = 0.0023$. Mean, Min, and Max plotted for each cell type.

almost 20% upon ARL16-myc expression, though this difference did not reach statistical significance (Figure 3C; $p > 0.05$). Expression of ARL16-myc in *Arl16* KO lines ($N = 2$ lines) resulted in a larger increase in ciliation, to levels approaching, and not statistically different from, those seen in WT cells also expressing ARL16-myc. Thus, expression of ARL16-myc reversed the decrease in ciliation observed in *Arl16* KO lines, supporting a role for ARL16 in ciliogenesis.

It was also evident that cilia in *Arl16* KO cells are longer than those in WT cells. Using the CiliaQ plug-in in FIJI (Hansen *et al.*, 2021), we measured cilia lengths after 48 h of serum starvation (Figure 3, D and E). On average, cilia in *Arl16* KO lines (5.09 μm) are ~90% longer than in WT (2.67 μm) cells, based on measurement of Ac-Tu staining.

To gain insights into likely causes of the deficits in ciliation in *Arl16* KOs, we screened markers of ciliogenesis for differences compared with WT MEFs. CEP164 recruitment to mother centrioles is an early step in ciliogenesis and required for cilium formation, while CP110 uncapping is a later step just before axoneme elongation (Cajanek and Nigg, 2014; Yadav *et al.*, 2016). We examined these proteins in WT and *Arl16* KO MEFs and found no statistically significant differences in either CEP164 recruitment or CP110 uncapping after 24 h of serum starvation (Supplemental Figure S4, A and B). Thus, we conclude that the defect in ciliogenesis observed in the *Arl16* KO MEFs is downstream of CP110 uncapping.

Ciliary rootlets surround the basal body, are important in centrosome cohesion, and often project a foot or extension that helps stabilize cilia (Yang *et al.*, 2002, 2005; Yang and Li, 2006; Hossain *et al.*, 2020). Thus, we stained WT and *Arl16* KO cells for rootletin, the primary component of rootlets. The absence of ARL16 strongly correlated with rootlet fragmentation (Supplemental Figure S4, C and D). However, in contrast to results observed in *Elmod2* KOs (Turn *et al.*, 2021), we did not observe an increase in centrosome separation in *Arl16* KOs, based on staining for γ-tubulin to mark centrosomes (Supplemental Figure S4E).

Arl16 KO leads to loss of several proteins from cilia

While cilia could be readily identified by Ac-Tu staining in all cells, ciliary ARL13B staining in *Arl16* KOs was dramatically reduced compared with that seen in WT cells (Figure 4, A and B). Because recruitment of ARL13B to cilia is required for ciliary accumulation of the other ciliary membrane proteins, specifically ARL3 and INPP5E (Gigante *et al.*, 2020), we assessed the endogenous levels and localizations of each of these proteins to the cilia of *Arl16* KO cells. We readily detected both ARL3 and INPP5E in cilia of control MEFs, but neither ARL3 nor INPP5E was found in *Arl16* KO cilia (Figure 4, C–F). Finally, we assessed the localization of the ciliary transmembrane protein adenylyl cyclase 3 (AC3) and found that AC3 is also lost from cilia of *Arl16* KOs.

To determine whether there was a generalized disruption in ciliary protein traffic, or a more specific loss related to ARL13B and ARL3, we expressed GFP-tagged somatostatin receptor (SSTR3-GFP) and assessed its ciliary localization in WT and *Arl16* KO MEFs. We observed similar SSTR3-GFP signal in the cilia of both *Arl16* KOs and WT controls (Supplemental Figure S4F). This suggests that the import of certain proteins is unaltered in cells lacking ARL16, though results from the exogenous expression of a tagged protein carry with it known caveats. We also examined a protein marker of the transition zone, CEP290. In both WT and *Arl6* KO cells, CEP290 localizes to the base of the cilium, indicating no evident defects in its localization upon ARL16 ablation (Supplemental Figure S4G). Thus, there is selective loss of a subset of ciliary proteins in cells lacking ARL16.

Shh signaling is defective in *Arl16* KO cells

In light of the loss of ARL13B from cilia in *Arl16* KO lines and its proven role in ciliary signaling yet ability to signal from outside cilia, we investigated whether ARL16 regulates Sonic Hedgehog (Shh) signaling (Caspary *et al.*, 2007; Larkins *et al.*, 2011; Bay *et al.*, 2018; Gigante *et al.*, 2020). Treatment of MEFs with Shh causes changes in the ciliary protein content, as well as processing of Gli transcription

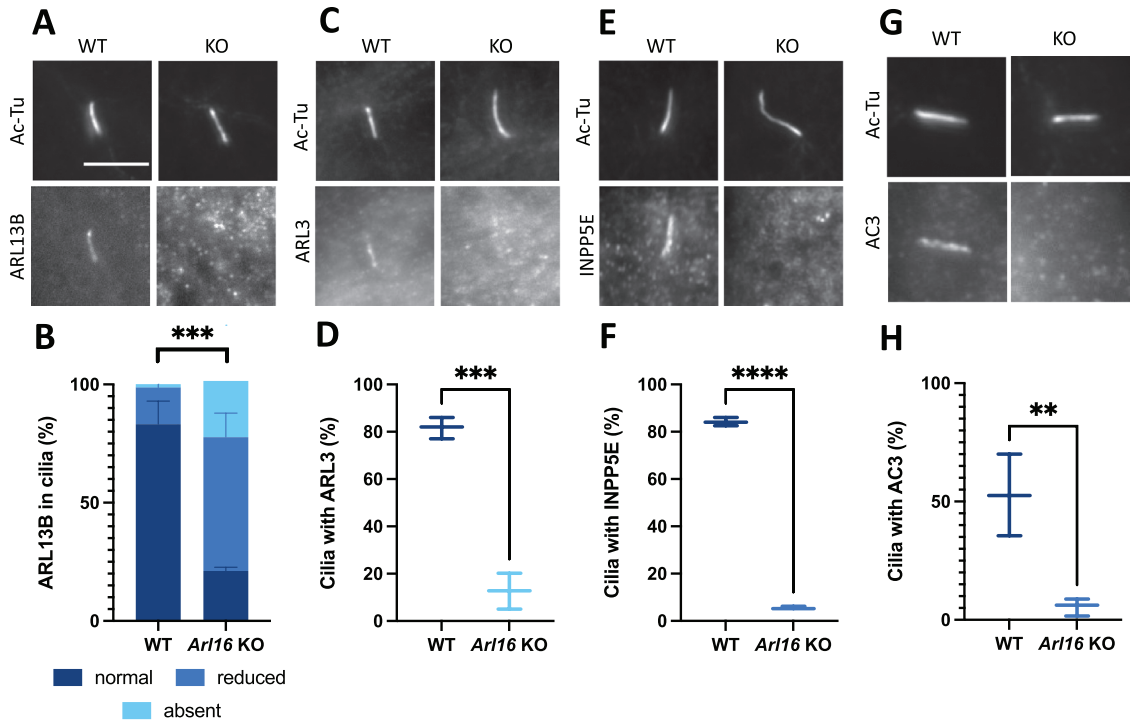

FIGURE 4: *Arl16* KO cells have reduced recruitment of several ciliary proteins. (A) ARL13B levels are reduced in *Arl16* KO cilia. Cells were serum starved for 48 h and stained for Ac-Tu and ARL13B. (B) Quantification of ARL13B-positive cilia in WT and *Arl16* KO lines. $N = 3 \times 100$ cilia $\times$ 5 KO lines or 2 WT lines. Cilia were identified using the Ac-Tu channel. The presence of ARL13B was scored by eye. Normal ARL13B staining was defined as staining that was readily apparent independent of the Ac-Tu channel. Reduced staining was apparent only after identification of the cilium using the Ac-Tu channel. Mean ± SD plotted. *t* test $p = 0.0002$. (C) ARL3 is reduced in *Arl16* KO cilia. Cells were serum starved for 48 h and stained for Ac-Tu and ARL3. (D) Quantification of C. $N = 3 \times 100$ cilia $\times$ 5 KO lines or 2 WT lines. Cilia were identified using the Ac-Tu channel. The presence of ARL3 was scored by eye. *t* test $p = 0.0002$. (E) INPP5E is absent from *Arl16* KO cilia. Cells were serum starved for 48 h and stained for Ac-Tu and INPP5E. (F) Quantification of E. $N = 3 \times 100$ cilia $\times$ 5 KO lines or 2 WT lines. Cilia were identified using the Ac-Tu channel. The presence of INPP5E was scored by eye. *t* test $p < 0.0001$. (G) AC3 is reduced in *Arl16* KO cilia. Cells were serum starved for 48 h and stained for Ac-Tu and AC3. (H) Quantification of G. $N = 3 \times 100$ cilia $\times$ 5 KO lines or 2 WT lines. Cilia were identified using the Ac-Tu channel. The presence of AC3 was scored by eye. *t* test $p = 0.0098$. Scale bar = 5 μm, 100× for all images. Mean, Min, and Max plotted for panels D, F, and H.

factors that ultimately results in changes in nuclear transcription, including that of *Ptch1* and *Gli1* mRNAs (Li *et al.*, 2021). Smoothened (SMO) dynamically localizes to the ciliary membrane in response to Shh stimulation, with SMO absent under control conditions and enriched upon stimulation with Shh ligand (Corbit *et al.*, 2005). Cells were treated with Shh-conditioned medium with serum starvation for 24 h and then stained for SMO. SMO is robustly increased in WT cilia but fails to do so in *Arl16* KOs (Figure 5, A and B).

To monitor transcriptional changes resulting from treatment of MEFs with Shh ligand, we performed quantitative PCR (qPCR) to measure *Ptch1* and *Gli1* mRNA levels (two well-known targets increased by Shh signaling) after Shh stimulation. We observed increases in the levels of each of these mRNAs in WT cells in response to Shh stimulation. In contrast, the responses were markedly blunted in *Arl16* KO cells (Figure 5C). Thus, ARL16 is also required for two well-characterized responses to Shh; SMO recruitment and transcriptional changes in target genes.

IFT140 is absent from cilia of *Arl16* KOs

We also analyzed the localization of several IFT components in *Arl16* KO cells. In WT cells, IFT140 is observed at the ciliary base and along the length of the cilium. In marked contrast, IFT140 associated with the cilium or base was strongly reduced in *Arl16* KO lines (Figure 6A). IFT140 is one of three core subunits of the IFT-A complex so its absence suggested the possibility of the absence of this entire complex. Surprisingly, when we examined another core IFT-A component, IFT144, we observed its presence in the cilium with no evidence of changes between WT and *Arl16* KO cells (Figure 6B). While optimizing staining protocols for IFT140, we found that IFT140 also localizes to rootlets, displaying strong overlap with rootletin staining in both WT and *Arl16* KO cells (Supplemental Figure S4H), even after fragmentation of rootlets in the KO cells.

We also examined the effects of *Arl16* KO on core components of the IFT-B complex, which consists of two core complexes (B1-1 and B1-2) and a peripheral complex (Yang and Huang, 2019; Quidwai *et al.*, 2021; Wang *et al.*, 2021). IFT81 (B1-1) and IFT88 (B1-2) localize along the length of the cilium and are often enriched at the base and tip in MEFs (Quidwai *et al.*, 2021). We observed no differences in the localization of either IFT88 or IFT81 in cilia of *Arl16* KO cells (Figure 6, C and D), with each of them localizing along the length of the cilium in both WT and KO cells. Therefore, we observed changes in the ciliary localization of a single IFT-A core component, IFT140, without apparent disruption of the other IFT-A or IFT-B components.

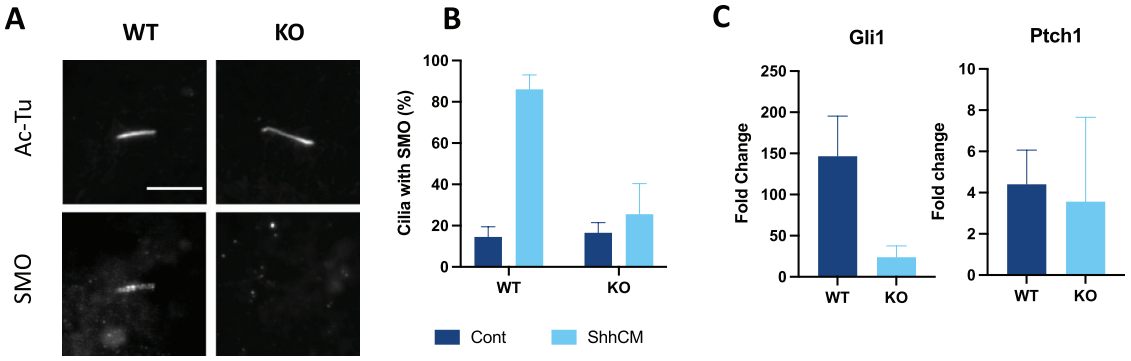

FIGURE 5: *Arl16* KO cells have defects in Hh signaling. (A) SMO is lost from cilia in *Arl16* KO lines. Cells were serum starved for 48 h and stained for Ac-Tu and SMO. Scale bar = 5 μm. (B) Quantification of A. $N = 2 \times 100$ cilia $\times$ 2 KO lines and 1 WT line per condition. Mean ± SD. (C) *Arl16* KO MEFs show reduced Shh-stimulated Gli1 and Ptch1 transcriptional response compared with WT cells. Cells were collected 24 h after Shh treatment, and levels of Gli1 and Ptch1 mRNA were determined using qPCR. Bar graphs indicate normalized mRNA expression with data presented as mean fold change ± SD. $N = 2$ WT lines and 4 KO lines.

IFT140 and INPP5E accumulate at the Golgi in *Arl16* KO cells

While we did not detect IFT140 in *Arl16* KO cilia, we noted instead that IFT140 accumulated in an intracellular membranous structure, which we identified as the Golgi by costaining with GM130 (Figure 7A). This Golgi staining of IFT140 was not evident in WT cells, and expression of ARL16-myc reversed the increased staining of IFT140 at Golgi (Figure 7B). The only other IFT protein previously known to be associated with the Golgi is IFT20 (Follit *et al.*, 2006; Keady *et al.*, 2011; Crouse *et al.*, 2014). Consistent with these earlier results, we found that in WT cells, IFT20 localizes to the Golgi and overlaps strongly with GM130 staining. We stained for IFT20 in *Arl16* KO cells and found no differences in its localization compared with WT cells (Figure 7C). IFT140 staining was prominent at the Golgi in the *Arl16* KOs. In contrast, we did not observe clear evidence of Golgi localization for any of the other IFT proteins examined, with less than 10% of both WT and KO cells having readily apparent Golgi staining of IFT144 or IFT88 (Figure 7, D and E). We also noted strong nuclear staining of IFT144, which has been reported previously by both this commercial antibody supplier and the Human Protein Atlas (https://www.proteinatlas.org/ENSG00000157796-WDR19/antibody#ICC). We then stained for several other Golgi markers (including β-COP, FAPP2, and GBF1) to assess whether overall Golgi structure may be altered in *Arl16* KO cells. Each of these proteins

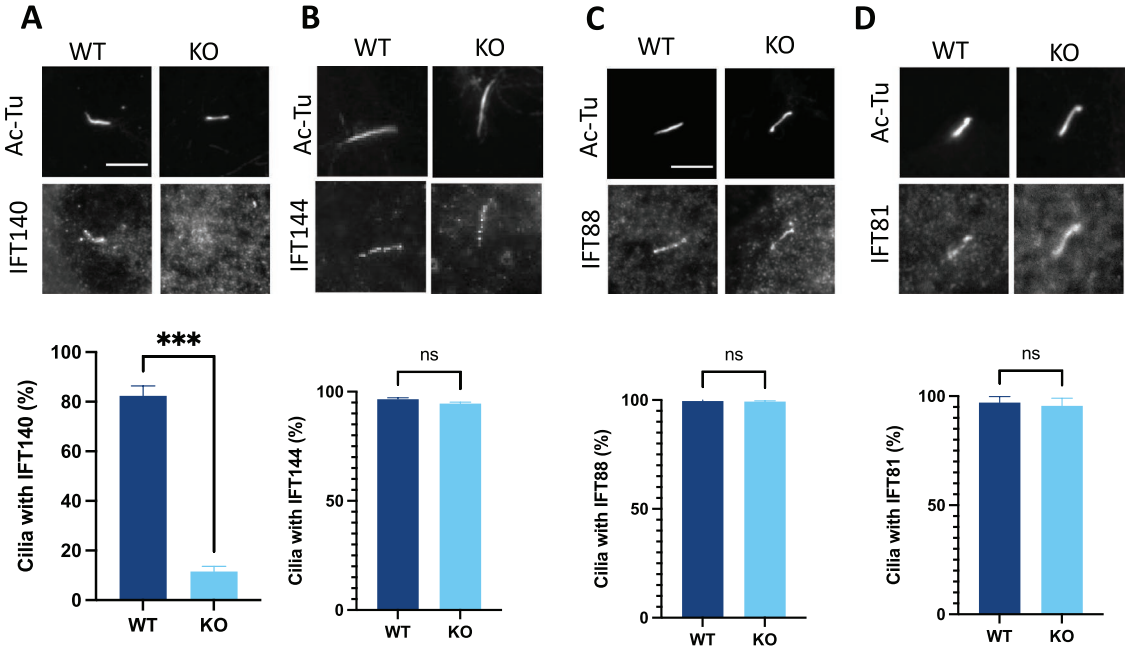

FIGURE 6: IFT140 is lost from cilia in *Arl16* KO cells, but other IFTs are unchanged. In each case, cells were serum starved for 48 h and then fixed and (top) stained with Ac-Tu and either IFT140 (A), IFT144 (B), IFT88 (C), or IFT81 (D) and imaged at 100× magnification. Quantification was performed in each case in duplicate for 100 cilia in WT ($N = 2$ cell lines) and *Arl16* KO lines ($N = 2$ lines). (A) IFT140 is lost from cilia in *Arl16* KO lines. (B) IFT144 staining in cilia is unchanged between WT and *Arl16* KO lines. $p = 0.1056$. (C) IFT88 is not altered in *Arl16* KO cilia from that in WT cells. $p = 0.6985$. (D) IFT81 is present in *Arl16* KO cilia as it is in WT cilia. $p = 0.6855$. Scale bar = 5 μm. Bar graphs represent mean ± SD.

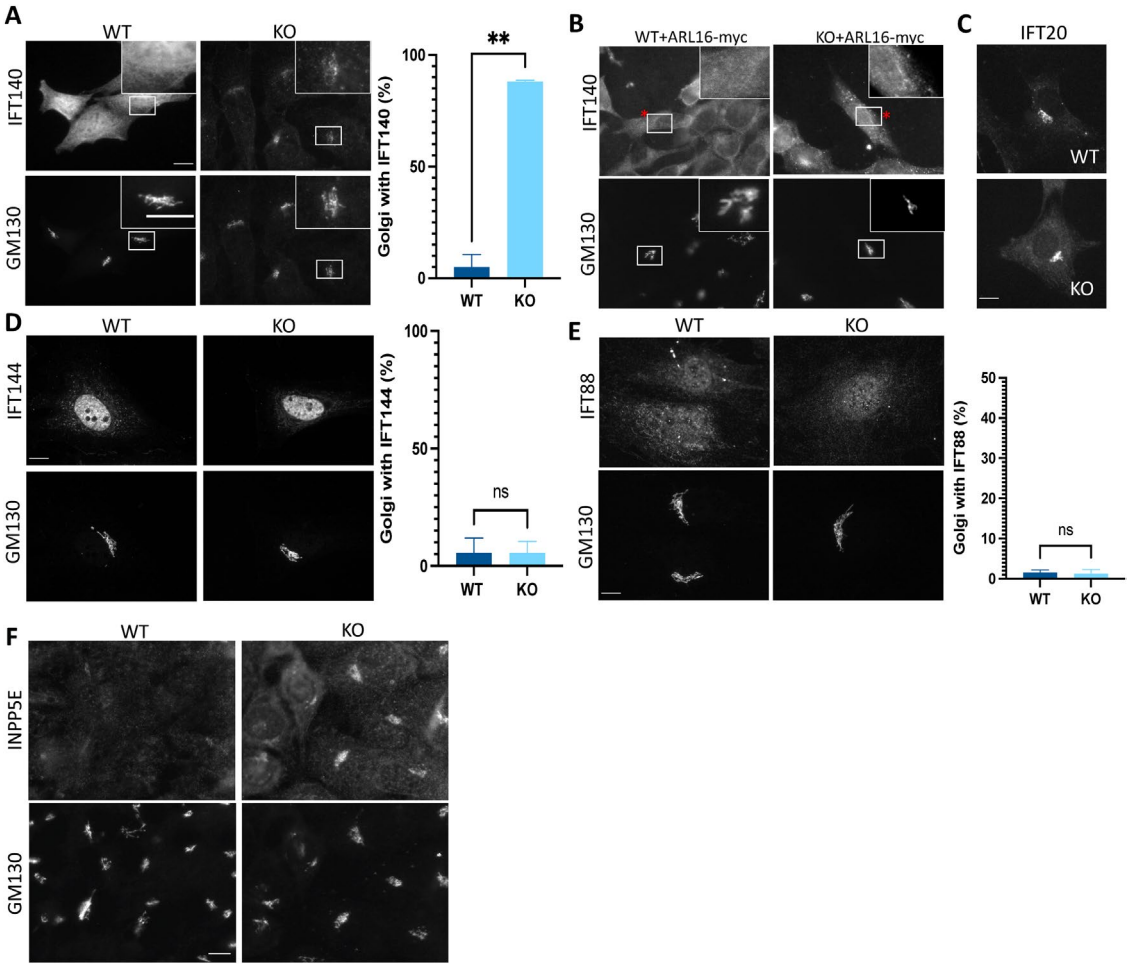

FIGURE 7: IFT140 and INPP5E accumulate at the Golgi of *Arl16* KO lines. (A) Cells were serum starved for 24 h and stained for IFT140 and GM130. IFT140 staining is diffuse in WT cells but clearly enriched at the Golgi in *Arl16* KOs. Bar graph shows quantification of percentage of Golgi with evident IFT140. $N = 2 \times 1$ line for WT and 2 lines for *Arl16* KO. (B) Expression of ARL16-myc reverses IFT140 accumulation in the Golgi. Cells were transfected with ARL16-myc, serum starved for 24 h, and stained for myc, GM130, and IFT140. Asterisks indicate transfected cell. (C) IFT20 localizes to Golgi indistinguishably in WT and *Arl16* KO cells. Cells were serum starved for 24 h and stained for IFT20. (D) IFT144 does not accumulate at Golgi in *Arl16* KOs. Cells were fixed and stained for IFT144 and GM130. Bar graph shows quantification of percentage of Golgi with evident IFT144. $N = 2 \times 1$ line for WT and 2 lines for *Arl16* KO. Note that the strong staining of nucleoplasm by the IFT144 antibody has been described previously and should not interfere with assessment of its presence at Golgi or in cilia. (E) IFT88 does not accumulate at Golgi in *Arl16* KOs. Cells were fixed and stained for IFT88 and GM130. Bar graph shows quantification of percentage of Golgi with evident IFT88. $N = 2 \times 1$ line for WT and 2 lines for *Arl16* KO. (F) Serum-starved cells were fixed and stained after 24 h and stained for INPP5E and GM130. INPP5E costaining with the Golgi marker GM130 is very strong while there was no evidence of changes in overall Golgi morphology. Bar graphs represent mean and SD. Scale bar = 10 μm throughout.

localizes to the Golgi in both WT and *Arl16* KO cells, and we observed no differences in Golgi morphology or intensity of any of these markers, based on visual inspection (Supplemental Figure S3B). Thus, while one component from each of the IFT-A and IFT-B complexes, IFT140 and IFT20, respectively, can be found at the Golgi, only IFT140 is increased in its abundance at the Golgi in *Arl16* KOs, while IFT20 appears to be a resident Golgi protein in both WT and *Arl16* KO MEFs.

Surprised by the accumulation of IFT140 in the Golgi in *Arl16* KOs, using a variety of staining protocols we assessed the Golgi localization of the other proteins that were lost from cilia to see whether any others were accumulating there. Staining of INPP5E at cilia is typically performed using paraformaldehyde (PFA) fixation, and under these conditions we observed it in cilia of WT lines but not in *Arl16* KO lines. However, after methanol fixation, we found that INPP5E staining increased at the Golgi in *Arl16* KO but not WT cells (Figure 7F). In contrast, neither ARL3 nor ARL13B was observed at the Golgi in either WT or *Arl16* KO lines under any conditions examined.

INPP5E but not IFT140 is lost from cilia and accumulates in the Golgi of *Pde6d* KOs

The phosphatidylinositol phosphate (PIP) 5′-phosphatase INPP5E is farnesylated at its C-terminus. As a result, its traffic to cilia is thought to be dependent on the prenyl-binding protein PDE6D (Cook *et al.*, 2000; Fansa *et al.*, 2016). The prevailing model postulates that PDE6D binds to INPP5E and carries it to the cilium, where it is released by ARL3 and retained by ARL13B (Humbert *et al.*, 2012; Thomas *et al.*, 2014; Kosling *et al.*, 2018). A high-throughput, yeast two-hybrid screen found that in addition to binding ARL3, PDE6D

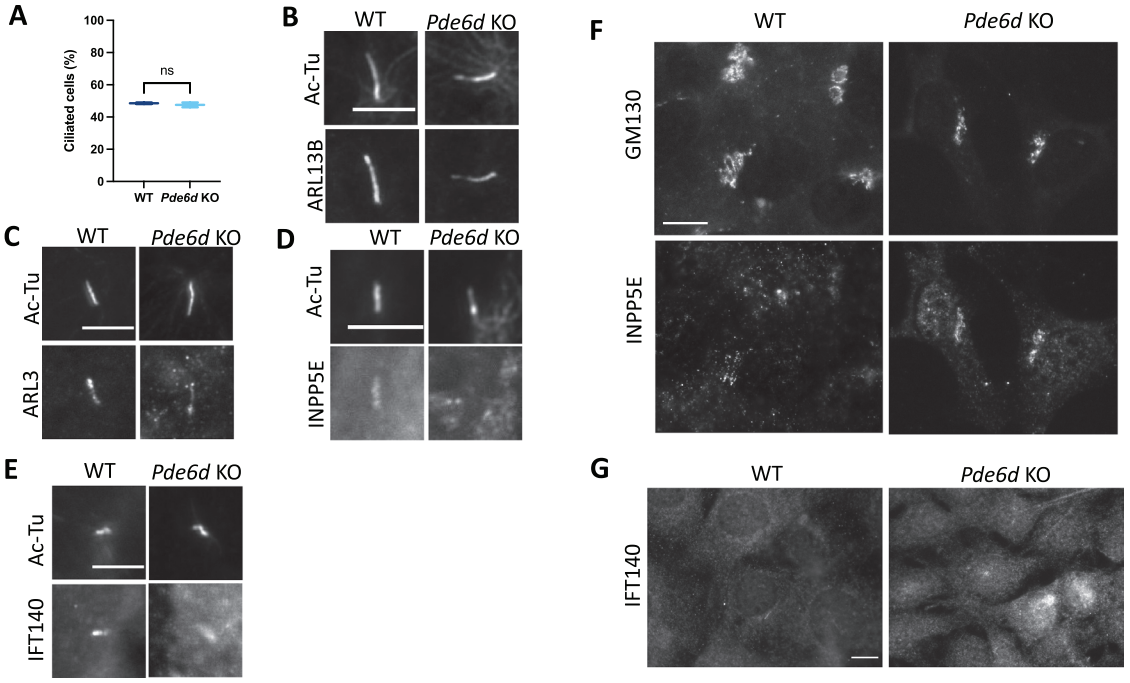

FIGURE 8: Cells deleted for *Pde6d* display no defects in ciliation but loss of INPP5E from cilia with its accumulation at Golgi. (A) Cells were serum starved for 24 h, stained for Ac-Tu, and scored for ciliation as described in *Materials and Methods*. $N = 2 \times 100$ cells for one WT and two KO lines. *t* test $p = 0.5918$. Mean, Min, and Max are plotted. (B) ARL13B and (C) ARL3 localize normally to *Pde6d* KO cilia. (D) INPP5E is lost from *Pde6d* KO cilia. (E) IFT140 localizes normally to cilia of *Pde6d* KO cells. (F) INPP5E is absent from cilia of *Pde6d* KO lines. Cells were serum starved for 24 h and stained for Ac-Tu and INPP5E. (G) INPP5E accumulates in the Golgi of *Pde6d* KO lines. Cells were serum starved for 24 h and stained for INPP5E and GM130. All images collected using 100× objective, and scale bars = 5 μm for B–E and 10 μm for F and G.

also binds ARL16 (Rolland *et al.*, 2014). Therefore, we generated *Pde6d* KO MEFs using the same protocols as those used to generate *Arl16* KOs (Supplemental Figure S5) to compare the phenotypes observed in the absence of *Pde6d* to those observed in the absence of *Arl16*. We generated five lines from two guide RNAs in which the *Pde6d* gene contained frame-shifting mutations (alleles of lines used in these studies are shown in Supplemental Figure S5B). Although PDE6D lacks motifs known to be essential for function, as are present in ARL16, we analyzed the potential for alternative splicing and use of downstream initiating methionines in our KO lines and conclude that it is highly unlikely that a functional protein is made in these cells (see Supplemental Figure S5) as >30% of the protein is absent in every case.

We then characterized the *Pde6d* KO lines for cilia number and protein composition. We observed no changes in the percentage of ciliated cells or length of cilia between *Pde6d* KO and WT cells (Figure 7, A and B). We also found no differences in the strength of staining of ARL13B or ARL3 in cilia of *Pde6d* KOs compared with WT cells (Figure 8, C and D). In contrast, when we examined ciliary staining of INPP5E, it was absent from *Pde6d* and *Arl16* KO lines while present in WT cells (Figure 8D). INPP5E was instead increased at the Golgi in *Pde6d* KO cells as in *Arl16* KO cells (Figure 7F).

We asked next whether IFT140 is also altered in *Pde6d* KO cells. We found that IFT140 localizes in *Pde6d* KO cilia at levels comparable to those in WT cilia and is not enriched at the Golgi (Figure 8G). Thus, while traffic of both IFT140 and INPP5E to cilia requires ARL16, only traffic of INPP5E appears to be dependent on PDE6D. These results are consistent with previous data showing PDE6D dependence of INPP5E traffic to cilia, likely the result of the prenylated INPP5E cargo binding the PDE6D shuttle. Further, these data suggest that IFT140 and INPP5E traffic to cilia via different pathways, each of which is dependent on, or regulated by, ARL16.

DISCUSSION

We used a combination of phylogenetic analyses, genome editing of MEFs, and cell biological approaches to identify the cellular functions of one of the last uncharacterized members of the mammalian ARF family of regulatory GTPases, ARL16. We identified a strong correlation between the presence of cilia and the presence of ARL16 in genomes across the eukaryotic spectrum, leading us to propose cilia as a major site of action. Consistent with our phylogenetics-based model, we found that ARL16 localizes to cilia and basal bodies in RPE and retinal photoreceptor cells, respectively. We generated *Arl16* KO MEF lines to identify gross changes in cellular biology resulting from its loss and to experimentally test its predicted role in one or more aspects of cilia. We found that the loss of ARL16 results in a reduction in ciliation, due to changes in a step downstream of CP110 uncapping. We also observed an increase in average ciliary length and a large decrease in the presence of ARL13B, ARL3, INPP5E, and IFT140 in cilia. However, we believe that the most important function of ARL16 in ciliary biology may lie in its role in the regulation of traffic of ciliary proteins from the Golgi to cilia. We found two such pathways that are compromised when cells lack ARL16, one used by IFT140 and another by INPP5E. Deficiency of either IFT140 or INPP5E at cilia is expected to spawn an unknown number of downstream phenotypes, as they are key regulators of traffic along cilia, of protein export (IFT140) and in the control of ciliary membrane phospholipid composition (INPP5E). We also provide data that support a model for ARL16 acting from multiple sites in cells, including basal bodies and Golgi. Thus, our findings

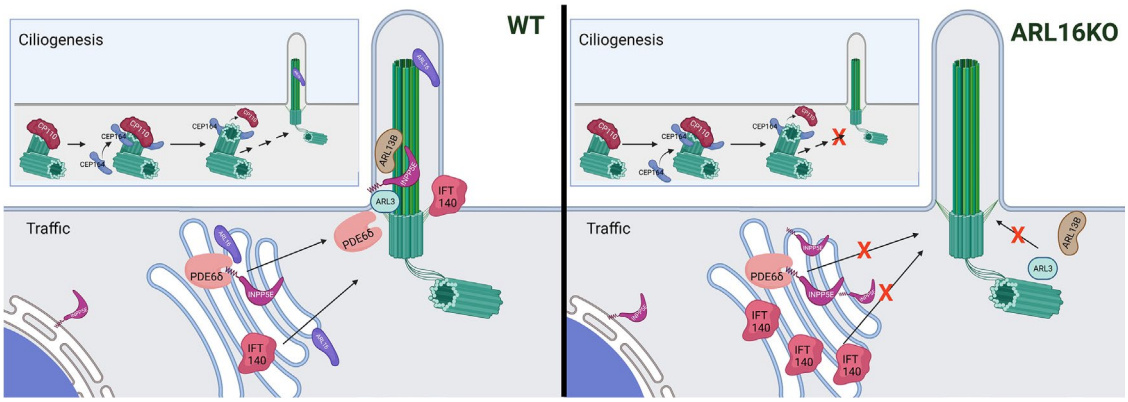

FIGURE 9: Model for ARL16 in ciliogenesis and Golgi to cilium traffic. *Ciliogenesis:* In WT cells induced to ciliate, CEP164 is recruited to mother centrioles as an early step in the ciliogenesis pathway, with later removal of the CP110 cap and extension of the axoneme. We propose that ARL16 acts after CP110 release to support ciliation such that in its absence ciliation is decreased and/or slowed. *Traffic:* In WT cells, INPP5E and IFT140 traffic through the Golgi during transit to cilia. ARL16 supports the export of INPP5E from the Golgi, likely working with PDE6D, to traffic INPP5E from the Golgi to the cilium, where it is released by ARL3 and retained by ARL13B. In contrast, IFT140 also requires ARL16, but not INPP5E, to be efficiently exported from the Golgi for transit to cilia. In addition, ARL3 and ARL13B fail to be recruited to or retained in cilia. Created with BioRender.com.

highlight both the importance of ARL16 to multiple processes and sites (summarized in the model shown in Figure 9) and also the challenges involved in future work aimed at identifying molecular mechanisms for each of its actions, as might be expected for such an ancient and highly conserved GTPase.

Phylogenetic analyses predict role(s) for ARL16 in ciliary biology

Our phylogenetic analyses demonstrated that ARL16 is restricted to ciliated taxa, similar to the three ARL GTPases previously shown to have ciliary-related roles: ARL3, ARL6, and ARL13. The phylogenetic profile (or phyletic pattern) of a gene can be an extremely informative resource providing evolutionary as well as functional insights. Genes encoding proteins that underpin the cilium are a particularly good illustration of this concept. Numerous genes subsequently demonstrated to encode proteins representing constituents of cilia or being critical for its biogenesis had been originally predicted as candidate "ciliary genes" based on searching for genes whose phylogenetic distribution correlates with the ability of the taxa to form cilia (Avidor-Reiss *et al.*, 2004; Li *et al.*, 2004; Merchant *et al.*, 2007; Nevers *et al.*, 2017). Other ciliary genes were discovered by ad hoc observations, as is the case of the Ras superfamily protein RJL proposed more than a decade ago to have a cilium-related role based on its phylogenetic distribution (Elias and Archibald, 2009) and confirmed as a regulator of ciliogenesis recently (Piette *et al.*, 2021).

ARL16 has been missed by most, if not all, previous comparative genomic screens for candidate ciliary taxa. One reason for this may stem from the high sequence divergence between ARL16 orthologues from distantly related eukaryotes, which might have resulted in the failure of commonly used, automated orthology prediction tools to recognize ARL16 genes in different species. Another confounding factor may be that the ARL16-cilium correlation is less conspicuous than in the case of many other ciliary genes in that it is missing in some ciliated species. That not all ciliary genes exhibit the same distribution pattern neatly correlating with the cilium is not unusual, as this cellular structure is highly malleable across species (Moran *et al.*, 2014). Perhaps most obvious is the difference between motile and primary cilia as the latter (analyzed in this study) lack a central pair of microtubules, dynein arms and radial spokes. This phenomenon is documented also by our phylogenetically broad survey of the distribution of ARL3, ARL6, and ARL13 (Figure 1; Supplemental Table S1). None is present in all cilium-building species, with ARL3 being the least frequently missing. Hence, the absence of ARL16 from various ciliated eukaryotes by itself does not undermine the prediction that this GTPase has a specific cilium-associated role. In fact, the restriction of ARL3, ARL6, ARL13, and ARL16 to cilium-building eukaryotes can be interpreted as evidence that the cilium-associated role of these proteins, established by studying a limited set of model organisms, is a general property across eukaryotes as a whole. A prediction we can draw then is that the potential nonciliary roles of these proteins are limited, making them dispensable whenever the cilium is lost. By extension, if ARL16 acts to regulate traffic from the Golgi, it may do so specifically in a Golgi–cilia pathway or for a subset of proteins destined for the cilium.

Deletion of *Arl16* causes a delay and overall decrease in ciliation yet increased ciliary length

We found that the percentage of cells that form cilia in response to serum starvation is reduced in *Arl16* KOs and that the affected step of ciliogenesis is downstream of CP110 uncapping of the basal body. It is by no means a complete defect in ciliation in the absence of ARL16. At later time points after serum starvation, *Arl16* KO cells achieve ciliation rates approaching those of WT MEFs and by 72 h show no statistically significant differences from WT. More-detailed tracking of centrioles and ciliation would be required to determine the precise step of ciliogenesis that is affected.

In addition, the cilia that do form in *Arl16* KOs are on average ~90% longer than WT cilia (Figure 3). While many things are known to result in shorter-than-average cilia (including the absence of ARL13B [Caspary *et al.*, 2007]), fewer things are known that increase ciliary length (Duran *et al.*, 2016; Wang *et al.*, 2021). One such regulator is Gli2-mediated autophagy of Ofd1 (Hsiao *et al.*, 2018), though we did not explore this pathway in the *Arl16* KOs.

We recently discovered that ciliary rootlets are linked to ciliogenesis and the ARF GAP ELMOD2 (Turn *et al.*, 2021). *Elmod2* KO resulted in rootlet fragmentation and increased centrosomal separation, each of which was reversed upon expression of fast-cycling ARL2 (Turn *et al.*, 2021).

However, while the loss of ARL16 results in rootlet fragmentation, there is no difference in centrosome separation between *Arl16* KO and WT cells. These somewhat surprising results both suggest a role for ARL16 in rootlet integrity and may also raise questions about the role of rootlets in centrosome cohesion.

ARL16 is required for localization of a subset of ciliary proteins

We found that ARL16 modulates multiple *aspects* of cilia. *Arl16* KO results in the marked reduction of several ciliary proteins including ARL13B, ARL3, and INPP5E. It is possible that the loss of some of these is a cascade effect beginning with the loss of ARL13B, as it has been shown to play important roles in binding and retention of both ARL3 and INPP5E in cilia (Schrick *et al.*, 2006; Kobayashi *et al.*, 2009; Wiens *et al.*, 2010; Ismail *et al.*, 2012; Mourão *et al.*, 2014; Gigante *et al.*, 2020). Farnesylated INPP5E is transported to the cilium by the carrier PDE6D where it is released by ARL3 (Fansa *et al.*, 2016; Stephen *et al.*, 2017). Therefore, the loss of INPP5E from cilia in *Arl16* KOs may result directly from the loss of ARL3 and/or ARL13B. We also found a reduction of AC3 in *Arl16* KO cilia, perhaps a result of altered ciliary PIP content due to the loss of INPP5E. Finally, changes in SMO recruitment (leading to defective Hh signaling) are likely due to the changes of these other ciliary proteins, each of which has been shown to regulate Hh signaling (Huangfu and Anderson, 2006; Humbert *et al.*, 2012; Placzek and Briscoe, 2018). Future experiments are likely to reveal additional changes in these cilia as a consequence of the loss of these or other proteins. For example, changes in ciliary INPP5E levels have been linked to changes in ciliary F-actin, release of ciliary vesicles (decapitation), and influence on cell cycle (Garcia-Gonzalo *et al.*, 2015; Phua *et al.*, 2017) that may also be sensitive to changes in ARL16 activities but will require additional study.

Golgi–cilia traffic is compromised by the lack of ARL16

The disruption of ciliary proteins often is accompanied by defects at the Golgi (Goncalves *et al.*, 2010; Dafinger *et al.*, 2011), and changes to the Golgi can affect ciliogenesis (Hurtado *et al.*, 2011; Greer *et al.*, 2014). While a few ciliary proteins also localize to the Golgi, (Follit *et al.*, 2006; Baron Gaillard *et al.*, 2011) the Golgi is close to the cilium both during ciliogenesis and after cilium maturation, suggesting that there is likely continuous transfer between these compartments (Poole *et al.*, 1997; Evans *et al.*, 2010). Some exclusive pathways transport specific cargoes from the Golgi to the cilium, including rhodopsin and PKD2 (Ward *et al.*, 2011; Kim *et al.*, 2014). Furthermore, recent work has highlighted a Golgi-to-cilium traffic pathway for ciliary membrane proteins that is regulated by IFT-A (Quidwai *et al.*, 2021).

IFT machinery is required for proper assembly and maintenance of primary cilia (Roepman and Wolfrum, 2007; Lechtreck, 2015; Nachury, 2018; Kannabiran, 2020). This machinery consists of two complexes; IFT-A, which is primarily responsible for retrograde transport from the cilium tip to the cell body, and IFT-B, which is critical for cilium assembly and anterograde transport. However, there is also mounting evidence of a role for IFT-A in anterograde transport as well (e.g., Mukhopadhyay *et al.*, 2010). Both IFT-A and -B are multisubunit complexes, with IFT-A containing six members (IFT140/144/139/122/121, and 43) and IFT-B further divided into two subcomplexes, a 10 subunit core (IFT-88/81/74/70/56/52/46/27/25, and 22) and a six subunit peripheral complex (IFT-172/80/57/54/38, and 20) (Jordan and Pigino, 2021). Little is known about where or how these complexes assemble in the cell before associating with cilia.

In *Arl16* KO cells, we found that the IFT-A core component IFT140 is lost from the cilium and accumulates at the Golgi. To date, the only other IFT protein known to localize to the Golgi is IFT20 (Follit *et al.*, 2006), which is anchored there by binding to GMAP210 (Follit *et al.*, 2008) and is required for opsin traffic from the Golgi to cilia (Keady *et al.*, 2011). Loss of either IFT20 or IFT140 causes similar degenerative phenotypes in both the cilium and retinal photoreceptor cells, and loss of either abrogates ciliogenesis, though phenotypes are more severe in the IFT20 deletion (Crouse *et al.*, 2014). However, several IFT subunits are associated with vesicular traffic functions in both ciliated and nonciliated cells (Yang and Huang, 2019). Interestingly, our data do not show changes in other examined IFT-A or -B components, leading us to conclude that IFT140 accumulation at Golgi is independent of the other IFT components and that IFT140 may be involved in a novel Golgi-to-cilium traffic pathway, or perhaps traffic to a distinct compartment at which assembly of the IFT-A complex takes place.

In addition to IFT140, INPP5E accumulates at the Golgi of *Arl16* KOs. Traffic of INPP5E has been extensively studied as mutations in it are associated with both Joubert and MORM ciliopathies. Our data here build upon that model and add to it. We show that in both *Arl16* KOs and *Pde6d* KOs, INPP5E accumulates at the Golgi. High-throughput screens also identified PDE6D as an interactor of ARL16 (Rolland *et al.*, 2014; Luck *et al.*, 2020). Therefore, we hypothesize that PDE6D picks up INPP5E at the Golgi to carry it to cilia in an ARL16-dependent manner.

Summary

This initial analysis of ARL16 identified roles in Golgi–cilia traffic that are likely linked with its effects on the control of ciliary length and ciliation itself, though acting at distinct sites. Clearly, substantially more work is required to identify each of the sites and mechanisms by which ARL16 acts. The current study used mammalian cell culture and CRISPR/Cas9-introduced mutations as a model system, though the presence of ARL16 in almost all ciliated eukaryotes should provide alternative systems that are predicted to yield additional insights into ARL16 actions. The use of CRISPR/Cas9-introduced indels and of tagged recombinant proteins for rescue or functional analyses each carries caveats important to solid interpretations. Further characterization of the cell lines described here and analyses of ARL16 biochemical activities will further strengthen current interpretations. Despite the limited number of ciliary proteins in our survey, we identified a number of proteins whose presence in cilia is compromised by the loss of ARL16. These proteins have been shown previously to play important roles in Shh signaling (ARL13B, ARL3, INPP5E), axoneme integrity (ARL13B), phospholipid metabolism (INPP5E), and retrograde intraflagellar traffic (IFT140) acting at or in cilia. Our findings of INPP5E and IFT140 accumulation at the Golgi in *Arl16* KOs and INPP5E but not IFT140 at the Golgi in *Pde6d* KOs support our model of ARL16 regulating two novel, independent traffic pathways from the Golgi to cilia. Finally, in a parallel study carried out in our lab we found phenotypes very similar to those reported here in *Arl16* KO lines when MEFs were deleted for either of the ARF/ARL GAPs ELMOD1 or ELMOD3 (Turn *et al.*, 2022). In addition, expression of ARL16-myc in *Elmod1* or *Elmod3* KO cells was able to reverse those phenotypes (Turn *et al.*, 2022), providing strong support for a model that includes these two proteins as acting in concert with ARL16 at the Golgi and in ciliary biology.

MATERIALS AND METHODS

Request a protocol through *Bio-protocol*.

Phylogenetic profiling of ARL3, ARL6, ARL13, and ARL16

The set of 114 eukaryotes previously analyzed for the composition of the ARF family gene complement (Vargová *et al.*, 2021) was expanded by 25 additional eukaryotes (see Supplemental Table S1), selected based on the following criteria: 1) representatives of those major eukaryotic lineages absent from the previous study (for the first time analyzing members of Hemimastigophora, Telonemia, Alveida, Rhodelphidia, and the CRUMs supergroup); 2) members of previously unsampled lineages known to have independently lost the cilium (Microsporidia, Myxozoa, Zygnematophyceae, Euglyphida); and 3) cilium-bearing close relatives of cilium-lacking taxa (e.g., the flagellated filasterean *Pigoraptor chileana* in contrast to the previously analyzed nonciliated filasterean *Capsaspora owczarzaki*). Available genomic or transcriptomic data from these eukaryotes (sources provided in Supplemental Table S2) were analyzed with BLAST searches (Altschul *et al.*, 1997) to identify putative orthologues of ARL3, ARL6, ARL13, and ARL16. Sets of protein sequences predicted based on genomic assemblies and transcriptome assembly contigs were searched with BLASTP and TBLASTN, respectively, using an ARF1 sequence as a query. Because ARL16 is rather distant from other ARF family members and is not always identified with ARF1 as the probing query, we performed parallel analyses starting with a reference ARL16 sequence as the BLAST query. Hits with the e-value ≤ 0.1 were retrieved and blasted (with BLASTP and BLASTX in the case of protein and nucleotide sequences, respectively) against an in-house database of Ras superfamily protein sequences including the curated set of ARF family sequences reported previously (Vargová *et al.*, 2021). Queries with the best 20 hits all corresponding to one of the four GTPases of interest (ARL3, ARL6, ARL13, and ARL16) were assigned as orthologues of the respective ARL protein, unless recognized as obvious contaminants from a different taxon (an issue sometimes happening in the case of transcriptome assemblies). Very rarely particular queries retrieved a set of 20 best hits consisting of a mixture of various ARF family members including some of the four focal GTPases. In all such cases the respective queries apparently corresponded to highly divergent genes with low sequence similarity to the canonical ARF family members and were hence discarded. We cannot exclude the possibility that some of these genes as well as some of the unclassified ARF family members from the previous analysis (Vargová *et al.*, 2021) are evolutionarily derived from ARL3, ARL6, ARL13, or ARL16 (i.e., being their orthologues or lineage-specific paralogues). However, in such cases their sequence divergence presumably entails a functional shift compared with canonical representatives of the four ARL paralogues, so failing to recognize their ultimate origin is unlikely to significantly impact the functional inferences from the phylogenetic distribution pattern of the four focal ARF family proteins. To avoid the possibility that any of the four GTPases is scored as missing for the given newly analyzed species only because of an accidental absence of the respective protein sequence resulting from inherently inaccurate genome annotation, we checked directly the genome assemblies with targeted TBLASTN searches and queries representing the ARL type not found in the predicted protein sequence set. All newly identified ARL3, ARL6, ARL13, and ARL16 sequences were manually checked and, if needed, the respective gene models were corrected to obtain accurate and complete protein sequences (the corrections are provided in Supplemental Table S2).

The distribution pattern of ARL3, ARL6, ARL13, and ARL16 in the total set of 139 eukaryotes was correlated with the presence of cilia. Each species was scored as ciliated or nonciliated (Figure 1; Supplemental Table S1) based on literature searches. A few apparently nonciliated taxa (the foraminiferan *Reticulomyxa filosa* and the green algae *Ostreococcus lucimarinus* and *Coccomyxa subelipsoidea*) possess subsets of genes encoding characteristic ciliary proteins, suggesting that these species may form cilia at unknown life stages or may have lost the ability to build these structures only recently (Glöckner *et al.*, 2014; Li *et al.*, 2020). The cilia in these species, if indeed formed, are presumably highly reduced, owing to the lack of genes encoding many core ciliary proteins. Consistent with this, these species either completely lack ARL3, ARL6, ARL13, and ARL16 or, in the case of *R. filosa*, possess only one of these ARLs (ARL6, together with an apparent pseudogene corresponding to ARL3; Supplemental Table S1). To account for the uncertain status of the cilium in these taxa, its presence was coded as ambiguous for the subsequent comparative analyses. The lack of evidence for the presence of ciliated stages in some poorly studied amoeboid protists (*Rigifila ramosa*, *Armaparvus languidus*) without genome sequence data should not be interpreted as evidence of absence of the cilium in these organisms, but the consistent lack of all four cilium-associated ARLs from the transcriptome data generated for them is consistent with the idea that all four, including ARL16, are not required when no cilium is formed. Hence, for the purpose of our correlation analysis, these species were scored as nonciliated. Finally, the pelagophyte alga *Aureococcus anophagefferens* was not reported to have cilia, but it possesses three out of the four cilium-associated ARLs (Supplemental Table S1) and was previously shown to encode various other ciliary proteins, so it likely forms a flagellated stage, most likely zoospores, like its relatives (for further details see Eliáš *et al.*, 2016). Hence, we scored it as a ciliated eukaryote.

The strength of the dependence of the presence of ARL16 on the presence of the cilium was formally tested using the pairwise comparisons algorithm (Maddison, 2000) implemented in the Mesquite package (Maddison and Maddison, 2021). A strictly bifurcating tree representing the phylogenetic relationships of the 139 taxa analyzed was constructed on the basis of previously published molecular phylogenetic and phylogenomic analyses. The somewhat contentious branching order of the main eukaryotic lineages was arbitrarily defined following the most recent and comprehensive phylogenomic study (Tice *et al.*, 2021), but alternative topologies at the base of the eukaryotic tree suggested by other studies would not impact the result of the correlation analysis, as they do not change the inferred positions of cilium and ARL16 loss events. The tree was loaded into Mesquite, and a two-character matrix was built following the character coding presented in Supplemental Table S1, with the character 1 corresponding to the cilium (three states: present, absent, and ambiguous) and the character 2 representing the presence or absence of ARL16. The Pairwise Comparison test was carried out with the "Most Pairs" option and 1000 pairings, and which gave the best tail p value range from 1.2×10^{-7} to 3.81×10^{-6} across all the pairings.

Reagents, antibodies, and plasmids

All chemicals used were purchased from commercial sources. The following antibodies were used in these studies: ARL16 (1:100; Sigma; HPA043711), acetylated tubulin (1:1000; Sigma; T5192), centrin clone 20H5 (1:1000; Sigma; 04-1624), polyclonal rabbit anti–centrin 3 (1:100 [Trojan *et al.*, 2008]), myc (1:1000; Abcam; ab9132), HSP60 (1:1000; Stressgen; ADI-SPA-807), GM130 (1:1000; BD/Transduction; 610823), tubulin (1:1000; EMD Millipore; MAB1864), β-COP (1:2000; ThermoFisher; PA1-061), FAPP2 (gift from Antonella De Matteis, Telethon Insitute of Genetics and Medicine [TIGEM], Pozzuoli [NA], Italy), GBF1 (1:200; BD; 612116), CP110 (1:100; Proteintech; 66448-1-ig), gamma tubulin (1:1000; Sigma T6557 or

Abcam ab11317), CEP164 (1:100; Santa Cruz; sc-515403), rootletin (1:1000; EMD Millipore; ABN1686), CEP290 (1:100; Proteintech; 22490-1-ap), NPHP4 (1:100; Proteintech; 13812-1-ap), IFT81(1:200; Proteintech; 11744-1AP), ARL13B (1:500; Proteintech; 17711-1-AP), ARL3 (1:100; R75448 [Cavenagh *et al*., 1994]), INPP5E (1:100; Proteintech; 17797-1-ap), AC3 (1:100; LSBio; LS-C204505/183274), SMO (gift from Kathryn Anderson, (Sloan Kettering Institute, New York City, NY [Ocbina *et al*., 2011]), GLI3 (1:1000; R&D Systems; AF3690), IFT140 (1:200; Proteintech; 17460-1-AP), IFT144 (1:100; Proteintech; 13647-1-AP), IFT88 (1:200; Proteintech; 13967-1-ap), and IFT20 (gift from Greg Pazour, University of Massachusetts Medical School, MA [Pazour *et al*., 2002]).

The plasmid directing expression of mouse ARL16-myc in mammalian cells was obtained by first having the open reading frame synthesized by GenScript and later using PCR to amplify this open reading frame with insertion of the C-terminal myc epitope (EQKLISEEDL) after a diglycine linker. The PCR product was ligated into pCDNA3.1 using *Kpn*I and *Xho*I sites, and the entire open reading frame was sequenced to confirm fidelity. The plasmid expressing SSTR3-GFP was a gift from Max Nachury, (University of California at San Francisco, CA (Marley *et al*., 2013).

Cell culture

All cells were maintained in DMEM (ThermoFisher #11965) supplemented with 10% fetal bovine serum (FBS) at 37°C and 5% CO_2. To induce ciliation, media was swapped with DMEM supplemented with 0.5% FBS for 48 h unless otherwise indicated. Cells were grown in the absence of antibiotics. Routine screening for mycoplasma contamination was performed using DNA staining.

CRISPR/Cas9

Genes of interest were disrupted in immortalized WT MEFs (American Type Culture Collection [ATCC] CRL-2991) with CRISPR/Cas9 gene editing, as previously described (Schiavon *et al*., 2019; Turn *et al*., 2020, 2021, 2022). Guide RNA sequences targeting the coding region of the gene were designed using Benchling (benchling.com/academic).

For *Arl16*, the guides used were Guide 2: GGAGAGCCCCCACCGACGCGG and Guide 3: CGGAGATGGCAAAGGCGACCT. For *Pde6d* the guides used were Guide 1: GCAAATGGAAAAATTCCGCC and Guide 3: CACCGCCTTCGGGATGCCGAAACA.

Double-stranded oligonucleotides of the guide sequences (with a substitution of a G for the first nucleotide to facilitate expression from the U6 promotor) were cloned into the pSpCas9(BB)-2A-Puro (PX459) V2.0 Vector (Addgene) at the *Bbs*I sites. Cells were transfected with the resulting plasmid with a 1:3 ratio of DNA (2 µg) to Lipofectamine 2000 (6 µg) for 4 h in OptiMEM, according to the manufacturer's instructions. Cells were then replated and allowed to recover overnight in DMEM with 10% FBS. Cells were then grown in 3 µg/ml puromycin for 4 d to enrich for transfected cells. Cells were then seeded into two 96-well plates at densities of 3–5 cells/well and monitored visually during growth. Wells containing more than single clones were discarded. Clones resulting from single cells were isolated, expanded, and cryopreserved. PCR primers were designed to amplify genomic DNA outside the target site to allow sequencing of genomic DNA to identify and verify frame-shifting mutations (indels). Inspection of the sequence data (e.g., any triplet peaks) was also used to ensure clonality, with ambiguous lines being discarded. Note that clones harboring no changes in the targeted region were often retained and are referred to as "CRISPR WT" cells as they had been through the transfection, selection, and cloning process as the null lines and serve as another control against off-target effects.

Sequences of alleles in each of the clones used in this study are shown in Supplemental Figure S3 (for *Arl16*) and Supplemental Figure S5 (for *Pde6d*). Note that almost all of the KO clones described have the same indel in both alleles. This was the result of selecting them on that basis as it simplified analyses of genomic sequencing data. The majority of clones sequenced had two different alleles.

Transfection

Cells were transfected with 4 µg of DNA:4 µl JetOPTIMUS transfection reagent (VWR; 76299-634) according to manufacturer guidelines in standard medium overnight. The next day, cells were replated on coverslips in standard medium and allowed to recover for 24 h. Cells were then serum starved for 24–72 h to induce ciliation before fixation.

Immunofluorescence

All cells were cultured on coverslips coated with Matrigel (BD Biosciences #356231).

PFA protocol. For the antibodies Ac-Tu, ARL13B, ARL3, INPP5E, γ-tubulin, SMO, and AC3), cells were fixed with 4% PFA in phosphate-buffered saline (PBS) prewarmed to 37°C on the benchtop for 15 min. Cells were permeabilized with 0.1% Triton X-100 in PBS for 10 min at room temperature. For Ac-Tu, ARL13B, and SMO, cells were blocked with 1% bovine serum albumin (BSA; Sigma #A3059) in PBS for 1 h. Primary antibodies were diluted in blocking solution and applied to cells at 4°C overnight. Cells were washed 4 × 5 min with PBS before incubation with secondary antibodies (1:1000; Alexa fluorophores; ThermoFisher) in blocking solution for 1 h at room temperature. Cells were washed 4 × 5 min with PBS before being mounted onto slides with MOWIOL. For ARL3, INPP5E, and AC3, a blocking solution of 10% FBS in PBS was used in place of 1% BSA.

Methanol protocol. For antibodies γ-tubulin, Ac-Tu, INPP5E at Golgi, CEP164, and CEP290, cells were fixed with methanol at –20°C for 10 min and washed in PBS with agitation. Cells were blocked with blocking buffer (PBS with 10% FBS) for 30 min at room temperature. Primary antibodies were diluted in blocking buffer and applied to the cells at 4°C overnight. Cells were washed 3 × 5 min with PBS with agitation before applying secondary antibody diluted 1:500 in blocking buffer for 1 h at room temperature. Cells were then washed and mounted as described above.

IFT protocol. The protocol for IFT staining (IFT140, IFT144, IFT88, and IFT81) was as follows. Immediately out of the incubator, cells were washed twice in PBS warmed to 37°C before fixation with 4% PFA in PHEM (60 mM PIPES, 22 mM HEPES, 10 mM ethylene glycol tetraacetic acid, 4 mM $MgSO_4$-$7H_2O$, pH 6.9) for 15 min at room temperature. Cells were washed twice with PBS and treated with 50 mM NH_4Cl twice for 15 min. Cells were washed again with PBS before permeabilization with 0.25% Triton X-100 in PBS for 10 min at room temperature. Cells were blocked with 10% FBS in PBS with 0.2% Tween 20 for 60 min at room temperature and then incubated with primary antibodies in 1% FBS in PBS with 0.025% Triton X-100 at room temperature for 1 h or at 4°C overnight. Cells were washed 4 × 10 min with PBS before incubation with secondary antibodies for 60 min at room temperature. Cells were rinsed with 0.25% Triton X-100 in PBS 5 × 10 min before being mounted as above.

Microscopy

Samples were visualized using an Olympus IX81 wide-field microscope, Hamamatsu C4742-95 digital camera, and Slidebook software; 100× objective (UPlanFI, 1.30 NA Oil) or Lionheart FX: Automated Microscope and Gen5 software; Olympus 60X Universal Plan Fluorite Dry Objective, 0.9 NA. Images were processed and analyzed using FIJI image analysis software. Any images appearing in the same panel of a figure were processed identically including objectives, acquisition settings, cropping, brightness adjustments, and any other processing settings.

Scoring of cell phenotypes

For all phenotypes that were scored, experiments were performed in triplicate and scored at least in duplicate as indicated in the corresponding figure legends. For percent ciliated cells, cilia were identified using Ac-Tu. For the presence of markers in cilia (ARL13B, ARL3, INPP5E, etc.), we binned them as either present (visible even without checking the Ac-Tu channel), reduced (present, but noticeable only upon switching to Ac-Tu channel), or absent (cannot be detected upon switching to Ac-Tu channel). For all ciliary phenotyping, Ac-Tu was used to define cilia. For centrosomal/basal body scoring, γ-tubulin was used as the standard comparison point. Finally, for Golgi staining/localization, GM130 was used to define the Golgi.

Human tissue

The human donor eye tissue applied in the present study was obtained 11.5 h postmortem from a female donor (#252-09), 65 yr of age without any underlying health conditions, from the Department of Ophthalmology, University Medical Center Mainz, Germany. The guidelines to the declaration of Helsinki (https://www.wma.net/policies-post/wma-declaration-of-helsinki-ethical-principles-for-medical-research-involving-human-subjects) were followed.

Immunohistochemistry of retinal sections

Human retinas were dissected from enucleated eyeballs, cryofixed in melting isopentane, and cryosectioned at –20°C in a cryostat (HM 560 Cryo-Star; MICROM) as previously described (Wolfrum, 1991; Karlstetter *et al.*, 2014). Sections (10 µm) were placed on poly-L-lysine–precoated coverslips and incubated with 0.01% Tween 20 in PBS for 20 min. After washing, the sections were flooded with blocking solution (0.5% cold-water-fish gelatin plus 0.1% ovalbumin in PBS) and incubated for at least 30 min followed by an overnight incubation with primary antibodies at 4°C in blocking solution (Trojan *et al.*, 2008). Washed cryosections were incubated with secondary antibodies conjugated to Alexa 488 or Alexa 568 (Invitrogen) in blocking solution and with 4,6-diamidino-2-phenylindole (Sigma-Aldrich) to stain the DNA of nuclei for 1.5 h at room temperature in the dark. After three washes in PBS, specimens were mounted in Mowiol 4.88 (Hoechst) and imaged using a Leica DM6000B deconvolution microscope.

Shh assay

Shh response was determined by measuring transcriptional changes in Gli1 and Ptch1 mRNA levels, as previously described (Mariani *et al.*, 2016). Cells were maintained in low-serum (0.5% FBS) media for 48 h either with or without Shh conditioning. RNA was prepared using the Qiagen RNeasy Kit with QIAshredder homogenizer columns, according to the manufacturer's protocols. RNA (200 ng) was used to generate cDNAs using BioRad iScript Reverse Transcription supermix. The following primers were used for qPCR:

Pold3 (housekeeping gene)

F: 5′-ACGCTTGACAGGAGGGGGCT-3′

R: 5′-AGGAGAAAAGCAGGGGCAAGCG-3′

Gli1

F: 5′-CTTCACCCTGCCATGAAACT-3′

R: 5′-TCCAGCTGAGTGTTGTCCAG-3′

Ptch1

F: 5′-TGCTGTGCCTGTGGTCATCCTGATT-3′

R: 5′-CAGAGCGAGCATAGCCCTGTGGTTC-3′

In brief, the cDNA was combined with primers and Bio-Rad Sso Advanced Universal SYBR Supermix according to the manufacturer's protocols (1725270). Samples were run on a Bio-Rad CFX96 Touch Real-Time PCR Detection System, and data were analyzed using Bio-Rad CFX Manager 3.1. The following program conditions were used: 95°C for 5 min; 45 cycles of 95°C for 15 s; 57°C for 30 s. Reactions were performed in technical duplicate on three biological replicates. Data were then analyzed by the ΔΔCT method and normalized to control WT levels for each transcriptional target (Livak and Schmittgen, 2001).

Reproducibility and statistics

All data were plotted using GraphPad Prism. Bar graphs represent the mean of the data, with error bars representing the SD, and box-and-whisker plots indicate the range of the data along with the median and upper/lower quartiles. *t* tests or one-way analysis of variance (ANOVA) tests were used to determine whether there were significant differences between test groups as indicated. Asterisks in a figure indicate statistical significance: $*p < 0.05$, $**p < 0.01$, $***p < 0.001$, $****p < 0.0001$. Actual *p* values are indicated in the figure captions.

ACKNOWLEDGMENTS

This work was supported by grants from the National Institutes of Health (NIH) (R35GM122568 to R.A.K., R35GM122549 to T.C., and F31HD096815 to S.I.D.), European Regional Development Funds (project OPVVV CZ.02.1.01/0.0/0.0/16_019/0000759 to M.E.), and the Czech Science Foundation (grant 20-27648S to M.E.). We thank Mike Murphy, RefSeq Curator (National Center for Biotechnology Information/National Library of Medicine/NIH) for clarification on mRNA variants of the human ARL16 mRNA. We also thank Nick Seyfried, Duc Duong, and the Emory Integrated Proteomics Core for their help with TMT-MS analyses of MEF lines and in particular Pritha Bagchi for help with analyses of the data, as well as Blaine Roberts for help with direct MS. We regret that due to the journal's limitation on words in the text we are unable to cite many important contributions in the primary literature.

REFERENCES

Altschul SF, Madden TL, Schaffer AA, Zhang J, Zhang Z, Miller W, Lipman DJ (1997). Gapped BLAST and PSI-BLAST: a new generation of protein database search programs. Nucleic Acids Res 25, 3389–3402.

Avidor-Reiss T, Maer AM, Koundakjian E, Polyanovsky A, Keil T, Subramaniam S, Zuker CS (2004). Decoding cilia function: defining specialized genes required for compartmentalized cilia biogenesis. Cell 117, 527–539.

Baron Gaillard CL, Pallesi-Pocachard E, Massey-Harroche D, Richard F, Arsanto JP, Chauvin JP, Lecine P, Kramer H, Borg JP, Le Bivic A (2011). Hook2 is involved in the morphogenesis of the primary cilium. Mol Biol Cell 22, 4549–4562.

Barratt J, Gough R, Stark D, Ellis J (2016). Bulky trichomonad genomes: encoding a Swiss army knife. Trends Parasitol 32, 783–797.

Bay SN, Long AB, Caspary T (2018). Disruption of the ciliary GTPase Arl13b suppresses Sonic hedgehog overactivation and inhibits medulloblastoma formation. Proc Natl Acad Sci USA 115, 1570–1575.

Bourne HR, Sanders DA, McCormick F (1991). The GTPase superfamily: conserved structure and molecular mechanism. Nature 349, 117–127.
Breslow DK, Hoogendoorn S, Kopp AR, Morgens DW, Vu BK, Kennedy MC, Han K, Li A, Hess GT, Bassik MC, *et al.* (2018). A CRISPR-based screen for Hedgehog signaling provides insights into ciliary function and ciliopathies. Nat Genet 50, 460–471.
Cajanek L, Nigg EA (2014). Cep164 triggers ciliogenesis by recruiting Tau tubulin kinase 2 to the mother centriole. Proc Natl Acad Sci USA 111, E2841–E2850.
Carter SP, Blacque OE (2019). Membrane retrieval, recycling and release pathways that organise and sculpt the ciliary membrane. Curr Opin Cell Biol 59, 133–139.
Caspary T, Larkins CE, Anderson KV (2007). The graded response to Sonic Hedgehog depends on cilia architecture. Dev Cell 12, 767–778.
Cavenagh MM, Breiner M, Schurmann A, Rosenwald AG, Terui T, Zhang C, Randazzo PA, Adams M, Joost HG, Kahn RA (1994). ADP-ribosylation factor (ARF)-like 3, a new member of the ARF family of GTP-binding proteins cloned from human and rat tissues. J Biol Chem 269, 18937–18942.
Chiang AP, Nishimura D, Searby C, Elbedour K, Carmi R, Ferguson AL, Secrist J, Braun T, Casavant T, Stone EM, Sheffield VC (2004). Comparative genomic analysis identifies an ADPribosylation factor-like gene as the cause of Bardet-Biedl syndrome (BBS3). Am J Hum Genet 75, 475–484.
Cook TA, Ghomashchi F, Gelb MH, Florio SK, Beavo JA (2000). Binding of the delta subunit to rod phosphodiesterase catalytic subunits requires methylated, prenylated C-termini of the catalytic subunits. Biochemistry 39, 13516–13523.
Corbit KC, Aanstad P, Singla V, Norman AR, Stainier DY, Reiter JF (2005). Vertebrate Smoothened functions at the primary cilium. Nature 437, 1018–1021.
Crouse JA, Lopes VS, Sanagustin JT, Keady BT, Williams DS, Pazour GJ (2014). Distinct functions for IFT140 and IFT20 in opsin transport. Cytoskeleton (Hoboken) 71, 302–310.
Dafinger C, Liebau MC, Elsayed SM, Hellenbroich Y, Boltshauser E, Korenke GC, Fabretti F, Janecke AR, Ebermann I, Nurnberg G, *et al.* (2011). Mutations in KIF7 link Joubert syndrome with Sonic Hedgehog signaling and microtubule dynamics. J Clin Invest 121, 2662–2667.
Davidson AE, Schwarz N, Zelinger L, Stern-Schneider G, Shoemark A, Spitzbarth B, Gross M, Laxer U, Sosna J, Sergouniotis PI, *et al.* (2013). Mutations in ARL2BP, encoding ADP-ribosylation-factor-like 2 binding protein, cause autosomal-recessive retinitis pigmentosa. Am J Hum Genet 93, 321–329.
Derelle R, Torruella G, Klimes V, Brinkmann H, Kim E, Vlcek C, Lang BF, Elias M (2015). Bacterial proteins pinpoint a single eukaryotic root. Proc Natl Acad Sci USA 112, E693–E699.
Dishinger JF, Kee HL, Jenkins PM, Fan S, Hurd TW, Hammond JW, Truong YN, Margolis B, Martens JR, Verhey KJ (2010). Ciliary entry of the kinesin-2 motor KIF17 is regulated by importin-beta2 and RanGTP. Nat Cell Biol 12, 703–710.
Duran I, Taylor SP, Zhang W, Martin J, Forlenza KN, Spiro RP, Nickerson DA, Bamshad M, Cohn DH, Krakow D (2016). Destabilization of the IFT-B cilia core complex due to mutations in IFT81 causes a spectrum of short-rib polydactyly syndrome. Sci Rep 6, 34232.
Elias M, Archibald JM (2009). The RJL family of small GTPases is an ancient eukaryotic invention probably functionally associated with the flagellar apparatus. Gene 442, 63–72.
Eliáš M, Klimeš V, Derelle R, Petrželková R, Tachezy J (2016). A paneukaryotic genomic analysis of the small GTPase RABL2 underscores the significance of recurrent gene loss in eukaryote evolution. Biol Direct 11, 5.
Evans RJ, Schwarz N, Nagel-Wolfrum K, Wolfrum U, Hardcastle AJ, Cheetham ME (2010). The retinitis pigmentosa protein RP2 links pericentriolar vesicle transport between the Golgi and the primary cilium. Hum Mol Genet 19, 1358–1367.
Fan Y, Esmail MA, Ansley SJ, Blacque OE, Boroevich K, Ross AJ, Moore SJ, Badano JL, MaySimera H, Compton DS, *et al.* (2004). Mutations in a member of the Ras superfamily of small GTP-binding proteins causes Bardet-Biedl syndrome. Nat Genet 36, 989–993.
Fansa EK, Kosling SK, Zent E, Wittinghofer A, Ismail S (2016). PDE6delta-mediated sorting of INPP5E into the cilium is determined by cargo-carrier affinity. Nat Commun 7, 11366.
Fisher S, Kuna D, Caspary T, Kahn RA, Sztul E (2020). ARF family GTPases with links to cilia. Am J Physiol Cell Physiol 319, C404–C418.
Flot JF, Hespeels B, Li X, Noel B, Arkhipova I, Danchin EG, Hejnol A, Henrissat B, Koszul R, Aury JM, *et al.* (2013). Genomic evidence for ameiotic evolution in the bdelloid rotifer Adineta vaga. Nature 500, 453–457.
Follit JA, San Agustin JT, Xu F, Jonassen JA, Samtani R, Lo CW, Pazour GJ (2008). The Golgin GMAP210/TRIP11 anchors IFT20 to the Golgi complex. PLoS Genet 4, e1000315.
Follit JA, Tuft RA, Fogarty KE, Pazour GJ (2006). The intraflagellar transport protein IFT20 is associated with the Golgi complex and is required for cilia assembly. Mol Biol Cell 17, 3781–3792.
Garcia-Gonzalo FR, Phua SC, Roberson EC, Garcia G 3rd, Abedin M, Schurmans S, Inoue T, Reiter JF (2015). Phosphoinositides regulate ciliary protein trafficking to modulate Hedgehog signaling. Dev Cell 34, 400–409.
Gigante ED, Caspary T (2020). Signaling in the primary cilium through the lens of the Hedgehog pathway. Wiley Interdiscip Rev Dev Biol 9, e377.
Gigante ED, Taylor MR, Ivanova AA, Kahn RA, Caspary T (2020). ARL13B regulates Sonic hedgehog signaling from outside primary cilia. eLife 9, e50434.
Glöckner G, Hülsmann N, Schleicher M, Noegel AA, Eichinger L, Gallinger C, Pawlowski J, Sierra R, Euteneuer U, Pillet L, *et al.* (2014). The genome of the foraminiferan Reticulomyxa filosa. Curr Biol 24, 11–18.
Goetz SC, Ocbina PJ, Anderson KV (2009). The primary cilium as a Hedgehog signal transduction machine. Methods Cell Biol 94, 199–222.
Goncalves J, Nolasco S, Nascimento R, Lopez Fanarraga M, Zabala JC, Soares H (2010). TBCCD1, a new centrosomal protein, is required for centrosome and Golgi apparatus positioning. EMBO Rep 11, 194–200.
Gotthardt K, Lokaj M, Koerner C, Falk N, Gießl A, Wittinghofer A (2015). A G-protein activation cascade from Arl13B to Arl3 and implications for ciliary targeting of lipidated proteins. eLife 4, e11859.
Greer YE, Westlake CJ, Gao B, Bharti K, Shiba Y, Xavier CP, Pazour GJ, Yang Y, Rubin JS (2014). Casein kinase 1delta functions at the centrosome and Golgi to promote ciliogenesis. Mol Biol Cell 25, 1629–1640.
Hansen JN, Rassmann S, Stüven B, Jurisch-Yaksi N, Wachten D (2021). CiliaQ: a simple, opensource software for automated quantification of ciliary morphology and fluorescence in 2D, 3D, and 4D images. Eur Phys J E 44, 18.
Hossain D, Shih SY-P, Xiao X, White J, Tsang WY (2020). Cep44 functions in centrosome cohesion by stabilizing rootletin. J Cell Sci 133, jcs239616.
Hsiao CJ, Chang CH, Ibrahim RB, Lin IH, Wang CH, Wang WJ, Tsai JW (2018). Gli2 modulates cell cycle re-entry through autophagy-mediated regulation of the length of primary cilia. J Cell Sci 131, jcs221218.
Huangfu D, Anderson KV (2006). Signaling from Smo to Ci/Gli: conservation and divergence of Hedgehog pathways from Drosophila to vertebrates. Development 133, 3–14.
Humbert MC, Weihbrecht K, Searby CC, Li Y, Pope RM, Sheffield VC, Seo S (2012). ARL13B, PDE6D, and CEP164 form a functional network for INPP5E ciliary targeting. Proc Natl Acad Sci USA 109, 19691–19696.
Hurtado L, Caballero C, Gavilan MP, Cardenas J, Bornens M, Rios RM (2011). Disconnecting the Golgi ribbon from the centrosome prevents directional cell migration and ciliogenesis. J Cell Biol 193, 917–933.
Ismail SA, Chen YX, Miertzschke M, Vetter IR, Koerner C, Wittinghofer A (2012). Structural basis for Arl3-specific release of myristoylated ciliary cargo from UNC119. EMBO J 31, 4085–4094.
Ivanova AA, Caspary T, Seyfried NT, Duong DM, West AB, Liu Z, Kahn RA (2017). Biochemical characterization of purified mammalian ARL13B protein indicates that it is an atypical GTPase and ARL3 guanine nucleotide exchange factor (GEF). J Biol Chem 292, 11091–11108.
Jacoby M, Cox JJ, Gayral S, Hampshire DJ, Ayub M, Blockmans M, Pernot E, Kisseleva MV, Compère P, Schiffmann SN, *et al.* (2009). INPP5E mutations cause primary cilium signaling defects, ciliary instability and ciliopathies in human and mouse. Nat Genet 41, 1027–1031.
Jordan MA, Pigino G (2021). The structural basis of intraflagellar transport at a glance. J Cell Sci 134, jcs247163.
Kannabiran C (2020). Review: intraflagellar transport proteins in the retina. Mol Vis 26, 652–660.
Karlstetter M, Sorusch N, Caramoy A, Dannhausen K, Aslanidis A, Fauser S, Boesl MR, NagelWolfrum K, Tamm ER, Jagle H, *et al.* (2014). Disruption of the retinitis pigmentosa 28 gene Fam161a in mice affects photoreceptor ciliary structure and leads to progressive retinal degeneration. Hum Mol Genet 23, 5197–5210.
Keady BT, Le YZ, Pazour GJ (2011). IFT20 is required for opsin trafficking and photoreceptor outer segment development. Mol Biol Cell 22, 921–930.
Kim H, Xu H, Yao Q, Li W, Huang Q, Outeda P, Cebotaru V, Chiaravalli M, Boletta A, Piontek K, *et al.* (2014). Ciliary membrane proteins traffic through the Golgi via a Rabep1/GGA1/Arl3-dependent mechanism. Nat Commun 5, 5482.
Kobayashi T, Hori Y, Ueda N, Kajiho H, Muraoka S, Shima F, Kataoka T, Kontani K, Katada T (2009). Biochemical characterization of missense

mutations in the Arf/Arl-family small GTPase Arl6 causing Bardet-Biedl syndrome. Biochem Biophys Res Commun 381, 439–442.
Kosling SK, Fansa EK, Maffini S, Wittinghofer A (2018). Mechanism and dynamics of INPP5E transport into and inside the ciliary compartment. Biol Chem 399, 277–292.
Lai CK, Gupta N, Wen X, Rangell L, Chih B, Peterson AS, Bazan JF, Li L, Scales SJ (2011). Functional characterization of putative cilia genes by high-content analysis. Mol Biol Cell 22, 1104–1119.
Larkins CE, Aviles GD, East MP, Kahn RA, Caspary T (2011). Arl13b regulates ciliogenesis and the dynamic localization of Shh signaling proteins. Mol Biol Cell 22, 4694–4703.
Lechtreck KF (2015). IFT—cargo interactions and protein transport in cilia. Trends Biochem Sci 40, 765–778.
Leipe DD, Wolf YI, Koonin EV, Aravind L (2002). Classification and evolution of P-loop GTPases and related ATPases. J Mol Biol 317, 41–72.
Li JB, Gerdes JM, Haycraft CJ, Fan Y, Teslovich TM, May-Simera H, Li H, Blacque OE, Li L, Leitch CC, *et al.* (2004). Comparative genomics identifies a flagellar and basal body proteome that includes the BBS5 human disease gene. Cell 117, 541–552.
Li L, Wang S, Wang H, Sahu SK, Marin B, Li H, Xu Y, Liang H, Li Z, Cheng S, *et al.* (2020). The genome of Prasinoderma coloniale unveils the existence of a third phylum within green plants. Nat Ecol Evol 4, 1220–1231.
Li X, Li Y, Li S, Li H, Yang C, Lin J (2021). The role of Shh signalling pathway in central nervous system development and related diseases. Cell Biochem Funct 39, 180–189.
Livak KJ, Schmittgen TD (2001). Analysis of relative gene expression data using real-time quantitative PCR and the 2(-delta delta C(T)) method. Methods 25, 402–408.
Luck K, Kim DK, Lambourne L, Spirohn K, Begg BE, Bian W, Brignall R, Cafarelli T, CamposLaborie FJ, Charloteaux B, *et al.* (2020). A reference map of the human binary protein interactome. Nature 580, 402–408.
Maddison WP (2000). Testing character correlation using pairwise comparisons on a phylogeny. J Theor Biol 202, 195–204.
Maddison WP, Maddison DR (2021). Mesquite: a modular system for evolutionary analysis. Version 3.70. http://www.mesquiteproject.org.
Mariani LE, Bijlsma MF, Ivanova AA, Suciu SK, Kahn RA, Caspary T (2016). Arl13b regulates Shh signaling from both inside and outside the cilium. Mol Biol Cell 27, 3780–3790.
Marley A, Choy RW, von Zastrow M (2013). GPR88 reveals a discrete function of primary cilia as selective insulators of GPCR cross-talk. PLoS One 8, e70857.
May-Simera H, Nagel-Wolfrum K, Wolfrum U (2017). Cilia—the sensory antennae in the eye. Prog Retin Eye Res 60, 144–180.
Merchant SS, Prochnik SE, Vallon O, Harris EH, Karpowicz SJ, Witman GB, Terry A, Salamov A, Fritz-Laylin LK, Marechal-Drouard L, *et al.* (2007). The Chlamydomonas genome reveals the evolution of key animal and plant functions. Science 318, 245–250.
Moran J, McKean PG, Ginger ML (2014). Eukaryotic flagella: variations in form, function, and composition during evolution. BioScience 64, 1103–1114.
Mourão A, Nager AR, Nachury MV, Lorentzen E (2014). Structural basis for membrane targeting of the BBSome by ARL6. Nat Struct Mol Biol 21, 1035–1041.
Mukhopadhyay S, Wen X, Chih B, Nelson CD, Lane WS, Scales SJ, Jackson PK (2010). TULP3 bridges the IFT-A complex and membrane phosphoinositides to promote trafficking of G protein-coupled receptors into primary cilia. Genes Dev 24, 2180–2193.
Nachury MV (2018). The molecular machines that traffic signaling receptors into and out of cilia. Curr Opin Cell Biol 51, 124–131.
Nachury MV, Mick DU (2019). Establishing and regulating the composition of cilia for signal transduction. Nat Rev Mol Cell Biol 20, 389–405.
Nevers Y, Prasad MK, Poidevin L, Chennen K, Allot A, Kress A, Ripp R, Thompson JD, Dollfus H, Poch O, Lecompte O (2017). Insights into ciliary genes and evolution from multi-level phylogenetic profiling. Mol Biol Evol 34, 2016–2034.
Ocbina PJ, Eggenschwiler JT, Moskowitz I, Anderson KV (2011). Complex interactions between genes controlling trafficking in primary cilia. Nat Genet 43, 547–553.
Pasqualato S, Renault L, Cherfils J (2002). Arf, Arl, Arp and Sar proteins: a family of GTP-binding proteins with a structural device for "front-back" communication. EMBO Rep 3, 1035–1041.
Pazour GJ, Baker SA, Deane JA, Cole DG, Dickert BL, Rosenbaum JL, Witman GB, Besharse JC (2002). The intraflagellar transport protein, IFT88, is essential for vertebrate photoreceptor assembly and maintenance. J Cell Biol 157, 103–113.
Phua SC, Chiba S, Suzuki M, Su E, Roberson EC, Pusapati GV, Schurmans S, Setou M, Rohatgi R, Reiter JF, *et al.* (2017). Dynamic remodeling of membrane composition drives cell cycle through primary cilia excision. Cell 168, 264–279.e215.
Piette BL, Alerasool N, Lin ZY, Lacoste J, Lam MHY, Qian WW, Tran S, Larsen B, Campos E, Peng J, *et al.* (2021). Comprehensive interactome profiling of the human Hsp70 network highlights functional differentiation of J domains. Mol Cell 81, 2549–2565.e2548.
Placzek M, Briscoe J (2018). Sonic hedgehog in vertebrate neural tube development. Int J Dev Biol 62, 225–234.
Poole CA, Jensen CG, Snyder JA, Gray CG, Hermanutz VL, Wheatley DN (1997). Confocal analysis of primary cilia structure and colocalization with the Golgi apparatus in chondrocytes and aortic smooth muscle cells. Cell Biol Int 21, 483–494.
Qiu H, Fujisawa S, Nozaki S, Katoh Y, Nakayama K (2021). Interaction of INPP5E with ARL13B is essential for its ciliary membrane retention but dispensable for its ciliary entry. Biol Open 10, bio057653.
Quidwai T, Wang J, Hall EA, Petriman NA, Leng W, Kiesel P, Wells JN, Murphy LC, Keighren MA, Marsh JA, *et al.* (2019). A WDR35-dependent coat protein complex transports ciliary membrane cargo vesicles to cilia. eLife 10, e69786.
Roepman R, Wolfrum U (2007). Protein networks and complexes in photoreceptor cilia. Subcell Biochem 43, 209–235.
Rolland T, Tasan M, Charloteaux B, Pevzner SJ, Zhong Q, Sahni N, Yi S, Lemmens I, Fontanillo C, Mosca R, *et al.* (2014). A proteome-scale map of the human interactome network. Cell 159, 1212–1226.
Satir P, Christensen ST (2007). Overview of structure and function of mammalian cilia. Annu Rev Physiol 69, 377–400.
Schiavon CR, Turn RE, Newman LE, Kahn RA (2019). ELMOD2 regulates mitochondrial fusion in a mitofusin-dependent manner, downstream of ARL2. Mol Biol Cell 30, 1198–1213.
Schrick JJ, Vogel P, Abuin A, Hampton B, Rice DS (2006). ADP-ribosylation factor-like 3 is involved in kidney and photoreceptor development. Am J Pathol 168, 1288–1298.
Sedmak T, Wolfrum U (2010). Intraflagellar transport molecules in ciliary and nonciliary cells of the retina. J Cell Biol 189, 171–186.
Smits AH, Ziebell F, Joberty G, Zinn N, Mueller WF, Clauder-Munster S, Eberhard D, Falth M, Savitski PG, Jakob P, *et al.* (2019). Biological plasticity rescues target activity in CRISPR knock outs. Nat Methods 16, 1087–1093.
Stephen LA, Elmaghloob Y, Ismail S (2017). Maintaining protein composition in cilia. Biol Chem 399, 1–11.
Sztul E, Chen PW, Casanova JE, Cherfils J, Dacks JB, Lambright DG, Lee FS, Randazzo PA, Santy LC, Schurmann A, *et al.* (2019). ARF GTPases and their GEFs and GAPs: concepts and challenges. Mol Biol Cell 30, 1249–1271.
Thomas S, Wright KJ, Corre SL, Micalizzi A, Romani M, Abhyankar A, Saada J, Perrault I, Amiel J, Litzler J, *et al.* (2014). A homozygous PDE6D mutation in Joubert syndrome impairs targeting of farnesylated INPP5E protein to the primary cilium. Hum Mutat 35, 137–146.
Tice AK, Zihala D, Panek T, Jones RE, Salomaki ED, Nenarokov S, Burki F, Elias M, Eme L, Roger AJ, *et al.* (2021). PhyloFisher: a phylogenomic package for resolving eukaryotic relationships. PLoS Biol 19, e3001365.
Trojan P, Krauss N, Choe HW, Giessl A, Pulvermuller A, Wolfrum U (2008). Centrins in retinal photoreceptor cells: regulators in the connecting cilium. Prog Retin Eye Res 27, 237–259.
Turn RE, East MP, Prekeris R, Kahn RA (2020). The ARF GAP ELMOD2 acts with different GTPases to regulate centrosomal microtubule nucleation and cytokinesis. Mol Biol Cell 31, 2070–2091.
Turn RE, Hu Y, Dewees SI, Devi N, East MP, Hardin KR, Khatib T, Linnert J, Wolfrum U, Lim MJ, *et al.* (2022). The ARF GAPs ELMOD1 and ELMOD3 act at the Golgi and cilia to regulate ciliogenesis and ciliary protein traffic. Mol Biol Cell 33, ar13.
Turn RE, Linnert J, Gigante ED, Wolfrum U, Caspary T, Kahn RA (2021). Roles for ELMOD2 and Rootletin in ciliogenesis. Mol Biol Cell 32, 800–822.
Vargová R, Wideman JG, Derelle R, Klimeš V, Kahn RA, Dacks JB, Eliáš M (2021). A eukaryote-wide perspective on the diversity and evolution of the ARF GTPase protein family. Genome Biol Evol 13, evab157.
Wang W, Jack BM, Wang HH, Kavanaugh MA, Maser RL, Tran PV (2021). Intraflagellar transport proteins as regulators of primary cilia length. Front Cell Dev Biol 9, 661350.
Ward HH, Brown-Glaberman U, Wang J, Morita Y, Alper SL, Bedrick EJ, Gattone VH 2nd, Deretic D, Wandinger-Ness A (2011). A conserved signal and GTPase complex are required for the ciliary transport of polycystin-1. Mol Biol Cell 22, 3289–3305.

Wiens CJ, Tong Y, Esmail MA, Oh E, Gerdes JM, Wang J, Tempel W, Rattner JB, Katsanis N, Park HW, Leroux MR (2010). Bardet-Biedl syndrome-associated small GTPase ARL6 (BBS3) functions at or near the ciliary gate and modulates Wnt signaling. J Biol Chem 285, 16218–16230.
Wingfield JL, Lechtreck KF, Lorentzen E (2018). Trafficking of ciliary membrane proteins by the intraflagellar transport/BBSome machinery. Essays Biochem 62, 753–763.
Wittinghofer A, Vetter IR (2011). Structure-function relationships of the G domain, a canonical switch motif. Annu Rev Biochem 80, 943–971.
Wolfrum U (1991). Distribution of F-actin in the compound eye of the blowfly, Calliphora erythrocephala (Diptera, Insecta). Cell Tissue Res 263, 399–403.
Yadav SP, Sharma NK, Liu C, Dong L, Li T, Swaroop A (2016). Centrosomal protein CP110 controls maturation of the mother centriole during cilia biogenesis. Development 143, 1491–1501.
Yang H, Huang K (2019). Dissecting the vesicular trafficking function of IFT subunits. Front Cell Dev Biol 7, 352.
Yang J, Gao J, Adamian M, Wen XH, Pawlyk B, Zhang L, Sanderson MJ, Zuo J, Makino CL, Li T (2005). The ciliary rootlet maintains long-term stability of sensory cilia. Mol Cell Biol 25, 4129–4137.
Yang J, Li T (2006). Focus on molecules: rootletin. Exp Eye Res 83, 1–2.
Yang J, Liu X, Yue G, Adamian M, Bulgakov O, Li T (2002). Rootletin, a novel coiled-coil protein, is a structural component of the ciliary rootlet. J Cell Biol 159, 431–440.
Yang Y-K, Qu H, Gao D, Di W, Chen H-W, Guo X, Zhai Z-H, Chen D-Y (2011). ARF-like protein 16 (ARL16) inhibits RIG-I by binding with its C-terminal domain in a GTP-dependent manner. J Biol Chem 286, 10568–10580.
Zhang T, Li S, Zhang Y, Zhong C, Lai Z, Ding J (2009). Crystal structure of the ARL2-GTP-BART complex reveals a novel recognition and binding mode of small GTPase with effector. Structure 17, 602–610.
Zhou C, Cunningham L, Marcus AI, Li Y, Kahn RA (2006). Arl2 and Arl3 regulate different microtubule-dependent processes. Mol Biol Cell 17, 2476–2487.